Khairul, M. A.; Doroodchi, Elham; Azizian, Reza; Moghtaderi, Behdad. 'The influence of different flow regimes on heat transfer performance and exergy loss of Al_2O_3/DI-water and CuO/DI-water nanofluids'. Published in *Applied Thermal Engineering* Vol. 122, p. 566-578 (2017)

Available from: http://dx.doi.org/10.1016/j.applthermaleng.2017.05.035

The influence of different flow regimes on heat transfer performance and exergy loss of Al_2O_3/DI-water and CuO/DI-water nanofluids

M.A. Khairul[1], Elham Doroodchi[2], Reza Azizian[3], Behdad Moghtaderi[1,]*

[1]Priority Research Centre for Frontier Energy Technologies and Utilisation, Chemical Engineering, Faculty of Engineering and Built Environment, The University of Newcastle, Callaghan, NSW 2308, Australia.

[2]Center for Advanced Particle Processing, Chemical Engineering, Faculty of Engineering and Built Environment, The University of Newcastle, Callaghan, NSW 2308, Australia.

[3]Advanced Thermal Solution Inc., 89-27 Access Road, Norwood 02062, MA, USA.

ABSTRACT

The convective heat transfer performance and energy efficiency of Al_2O_3/DI-water and CuO/DI-water nanofluids flowing through a straight vertical tube was experimentally studied for laminar, transitional and turbulent flow regimes. A circulating rig was built to conduct the experiments at constant heat flux and various particle concentrations of 0.20, 0.30 and 0.50 wt% for both of the nanofluids. Specifically, the influence of transitional flow on the heat transfer coefficient, friction factor and exergy loss of the nanofluids were analysed. An improvement in the convective heat transfer coefficient for both Al_2O_3 and CuO nanofluids was found when compared to DI-water at all flow conditions. The maximum enhancement of 25% in heat transfer coefficient was observed for the 0.50 wt% CuO nanofluid. At laminar flow conditions, the pumping power was similar for all the working fluids, however, it was more pronounced under the transitional and turbulent flow regimes with an average of 3.9% increment in pumping power for CuO nanofluids. Besides, the highest energy efficiency was found to be 84% with 12.8% and 3.45% average reduction in exergy loss for 0.50 wt% of CuO/DI-water nanofluid in laminar and turbulent flow conditions, respectively. New

[*] Corresponding author: Tel: +61 2 4033-9062, Fax: +61 2 4033-9095
Email: Behdad.Moghtaderi@newcastle.edu.au (Attn: Professor Behdad Moghtaderi)

correlations are also proposed based on the experimental results, which can predict the Nusselt number for both nanofluids in laminar and turbulent flow regimes with high accuracy. It was concluded that the copper oxide nanofluid might be a good candidate for heat transfer applications because of their superior heat transfer performance in comparison to other classes of nanofluids as well as DI-water. Therefore, these types of nanofluids can be used to improve the heat transfer in many industrial sectors with more effective way.

Keywords: heat transfer performance; transitional flow; energy efficiency; exergy loss; input power, new correlations for Nu

Nomenclature

c_p	specific heat capacity (*J/kg K*)	Greek symbols	
C	heat capacity rate (*W/K*)	φ	particles weight fraction (*%*)
D	tube diameter (*m*)	ρ	density (kg/m^3)
E_{loss}	exergy loss (*J*)	μ	viscosity ($N\ s/m^2$)
f	friction factor	β	thermal expansion coefficient (K^{-1})
Gr	Grashof number	η	energy efficiency
g	acceleration of gravity (m/s^2)	Subscripts	
h	heat transfer coefficient ($W/m^2\ K$)	b	bulk
k	thermal conductivity (*W/m.K*)	bf	base fluid
L	length of the test section (*m*)	e	environment
$\dot{m}$	mass flow rate (*kg/s*)	i	inner
Nu	Nusselt number	in	input
Pr	Prandtl number	lam	laminar flow
ΔP	pressure drop (*Pa*)	nf	nanofluids
P_p	pumping power (*W*)	np	nanoparticles
q''	heat flux based on thermal power (W/m^2)	o	outer
Q	thermal power (*W*)	out	output
Re	Reynolds number	w	wall
S	tube circumference (*m*)	x	local
T	temperature (*K*)	$trans$	transitional flow
v	velocity (*m/s*)	$turb$	turbulent flow

1. Introduction

There has been a significant rise in the development in the electronic, communication and computing technologies over the last decade. This type of advancement demands decreases in size and while also endeavouring to enhance storage as well as operational capacities. Therefore, improvements in the cooling systems utilised is a critical issue. It is well known that the cooling rate can be enhanced by increasing the heat transfer surface area, but this technique involves an undesirable rise in the size of the heat transfer system [1, 2].

Currently, different studies have been completed on microscale heat transfer; however, the conventional fin and microchannel technologies seem to be inadequate for future generation technologies [3]. Typically water, ethylene glycol and engine oil are used as conventional heat transfer fluids in heat exchanger system which have demonstrate considerably poor heat transfer performance [4, 5]. The thermal conductivity of a fluid plays a vital role in the development of energy efficient heat transfer system and making them more effective and compact in size. The concept of employing particulate dispersions as a method for enhancing the thermal conductivity is not a new discovery. Theoretically, Maxwell proposed the concept of increased electrical conductivity of fluids with particulate dispersions over 120 years ago [6]. After this theory, many investigations have been conducted on millimetre and micrometre sized particles dispersed in various fluids [7]. Application of such coolants to real systems proved difficult due to the inherent inability to keep these particles dispersed in fluids and the resultant settling and clogging potential. Therefore, these fluids have never seriously been considered for industrial applications.

Nano-scale particles (<100 nm) in the conventional fluids exhibit promising application in science and technology due to their remarkable physicochemical properties. The most notable features of this type of fluid/particle mixture includes improved heat transfer performance, such as improvements to the thermal conductivity and convective heat transfer coefficient without significant changes to chemical and physical properties with less penalty of pressure drop and friction factor [8, 9]. These fluids are termed 'nanofluids', and are considered as the most promising heat transfer fluids for the future generation.

Pak and Cho [10] studied TiO_2/water and γ-Al_2O_3/water nanofluids for fully turbulent flow regimes, and found 45% enhancement in the heat transfer coefficient for γ-Al_2O_3/water nanofluids with volume fraction of 1.34%. But, for TiO_2/water nanofluids, the improvement in heat transfer was less in comparison to γ-Al_2O_3/water nanofluids at the same volume fraction of nanoparticles. Xuan and Li [11] examined the flow feature and convective heat transfer performance of CuO/water nanofluids with nanoparticle volume fractions varying between 0.3% and 2% in the turbulent flow regime. The maximum increases in heat transfer was more than 39% at 2 vol% of nanofluid. Sharma et al. [12] analysed the heat transfer coefficient as well as friction factor of Al_2O_3/water nanofluids in the transitional flow regime with a twisted tape insert in the test section. The highest heat transfer coefficient was found to be 23.70% at 0.10 vol% of nanoparticles when compared with water. Moreover, the value of friction factor of the nanofluid with twisted tape was 1.21 times higher than that the value of water flowing through a plain tube. A comparison study on the thermal characteristics of Al_2O_3/water and CuO/water nanofluids in transitional flow regime has been done by Suresh et al [13]. They concluded that CuO/water nanofluid with helical screw tape inserts gave better thermal performance in comparison to Al_2O_3/water nanofluid.

Table 1 shows the comparison of previous studies found in the available literatures. It summarises the types of nanofluids with different flow ranges as well as the percentage of changes in their heat transfer performance with respect to water.

Table 1: Comparison of previous study in terms of type of nanofluids, particle loading, flow range, and outcome in comparison to pure water.

Author	Type of nanofluid	Nanoparticle loading (%)	Flow range	Result*
Naik et al. [14]	CuO/water	0.10 and 0.30 vol%	Turbulent	17.62% enhancement in Nusselt number for 0.30 vol% 1.149 times higher friction factor for 0.30 vol%
Fotukian and Esfahany [15]	CuO/water	>0.24 vol%	Turbulent	25% increase in heat transfer coefficient 20% penalty in pressure drop.
Fotukian and Esfahany [16]	γ-Al_2O_3/water	>0.20 vol%	Turbulent	48% improvement in heat transfer coefficient for 0.054 vol% 30% enhancement in pressure drop for 0.135 vol%
Anoop et al. [17]	γ-Al_2O_3/water	1.0, 2.0, 4.0, and 6.0 wt%	Laminar	25% enhancement in heat transfer coefficient at 4 wt% for 45 nm 11% enhancement in heat transfer coefficient at 4 wt% for 150 nm
Kim et al. [18]	Al_2O_3/water	3.0 vol%	Laminar and turbulent	15% and 20% improvement in convective heat transfer coefficient for laminar and turbulent flow, accordingly
Wen and Ding [19]	γ-Al_2O_3/water	1.60 vol%	Laminar	47% maximum increase in local heat transfer coefficient
Heris et al. [20]	Al_2O_3/water and CuO/water	0.20-3.0 vol%	Laminar	1.29 and 1.23 times increase in the ratio of the experimental heat transfer coefficient to the theoretical result for Al_2O_3/water and CuO/water, accordingly at 2.5 vol%
Meyer et al. [21]	MWCNT/water	0.33, 0.75 and 1.0 vol%	Laminar and turbulent	1.6% decrease in heat transfer at 0.33 vol% for laminar flow 2.2% and 2.3% heat transfer enhancement at 0.75 and 1.0 vol% for laminar flow. 9.7%, 23.5% and 33.2% enhancement in heat transfer with 0.33, 0.75 and 1.0 vol%, respectively for turbulent flow

*% of enhancement/decrease with respect to water

From the above literature review, most of the studies have been completed in the laminar [22-25] or highly turbulent flow ranges [3, 18, 22, 26] and a very small number of works have been considered in the transitional flow regime [27]. Whenever planning to design heat transfer equipment in the last decade, usually the transitional flow region is avoided because of the associated uncertainty and flow instability. Pressure variation is also found in this regime, and this may involve a significant pumping power enhancement. However, there are lots of advanced heat transfer techniques being introduced in heat exchanging system, as a result the mass flow rate has been reduced gradually over the past years to fulfil required heat transfer. Now-a-days, a noticeable amount of heat transfer equipment operates in the transitional flow range or close to it. Hence, more research is necessary to define the heat transfer of nanofluids in the transitional flow region. Olivier and Meyer [28], and Meyer and Olivier [29] studied the heat transfer performance of nanofluids in the transitional flow regime in terms of heat transfer coefficients and pressure drops. They noticed that there was a smooth transition from the laminar to turbulent flow regime, and that the pressure drop and heat transfer properties were stable.

Stability of the nanoparticles is a vital concern in nanofluid research, as achieving a well suspended nanofluid on the long term remains a big challenge. Attempts to overcome this problem include controlling the surface potential by changing the types and weight concentrations of different surfactant additions, and as a result, this usually enables heat transfer enhancement of nanofluids [30]. However, very little research have been carried out to understand the influence of anionic surfactants on heat transfer performance of nanofluids [30]. Furthermore, most of the studies have been limited to thermal conductivity, viscosity, heat transfer coefficient, and pressure loss of nanofluids, and while the analyses of energy efficiency, exergy loss of nanofluids have been neglected [31]. Exergy is defined as the maximum available work in a substance during a process that brings the system back to equilibrium with a heat reservoir. Exergy is that portion of energy that can transform to another form of energy. Analysis of exergy is necessary for improving the energy efficiency and minimizing losses, because it quantifies the location, type, and magnitudes of waste and losses [32, 33].

Thus, the scope of the present study is to investigate the heat transfer performance of Al_2O_3/deionised (DI)-water and CuO/DI-water nanofluids with various nanoparticles weight concentration from 0.20 to 0.50% at laminar, turbulent and transitional flow regions. Specifically, the effects of different Reynolds number as well as input power on the convective heat transfer coefficient, energy efficiency and exergy loss of two different types of nanofluids are studied. Then the experimental results are compared with the results of DI-water and existing correlations available in the literatures [34-38], and four new correlations are proposed to predict the Nusselt number of nanofluids for laminar and turbulent flow regimes.

2. Experimental procedure and validation

2.1. Experimental set-up

Fig. 1 presents a schematic diagram of the experimental setup used in this research. The closed-loop flow system was installed with a flow meter, miniature gear pump, coil heat exchanger, pressure transmitter, DC power supply and thermocouples. The test section in the experimental rig consisted of a stainless steel tube of an outer diameter of 6.35 mm, inner diameter of 4.57 mm, and a length of 1 m. Eleven T-type thermocouples with bare wire configuration were placed evenly along the outer wall of the tubing to measure the wall temperature of the test section. Two T-type thermocouples with a MIMS (mineral insulated metal sheathed) configuration were used to measure the bulk inlet and outlet temperatures of the fluid, rather than the temperature of the test section directly, therefore, it will avoid any influence that may occur across the test section due to heat flux. The thermocouples were calibrated with a maximum standard deviation of 0.5 ºC.

A heat flux was supplied throughout the experimental test section by employing a SPV-1500 single output power supply with a rated power of 1500 W, current range of 0 to 125 A and DC output voltage is 12 V. The load regulation of the output power supply was ±0.5%. The copper electrode blocks were used to provide power into the test section, which were capable of delivering resistive heating. Ceramic fibre insulation, 12.5 mm in thickness, was applied across the test section to minimise heat loss.

For each run, the heat transfer fluid either a nanofluid or DI-water was poured into the stainless steel pipe through the storage tank. A miniature gear pump (12 Volt DC) was utilised to circulate the working fluid at a constant flow rate in the closed-loop flow system. The volumetric flow rate of the working fluid was measured using an ultrasonic flow meter (Cynergy- UF08B) with a maximum flow rate of 8 L/min. The accuracies of the flow meter are 5% and 3% of the reading at flow rates 0.1-0.4 L/min and 0.4-8 L/min, respectively, and the response time is better than 0.1s.

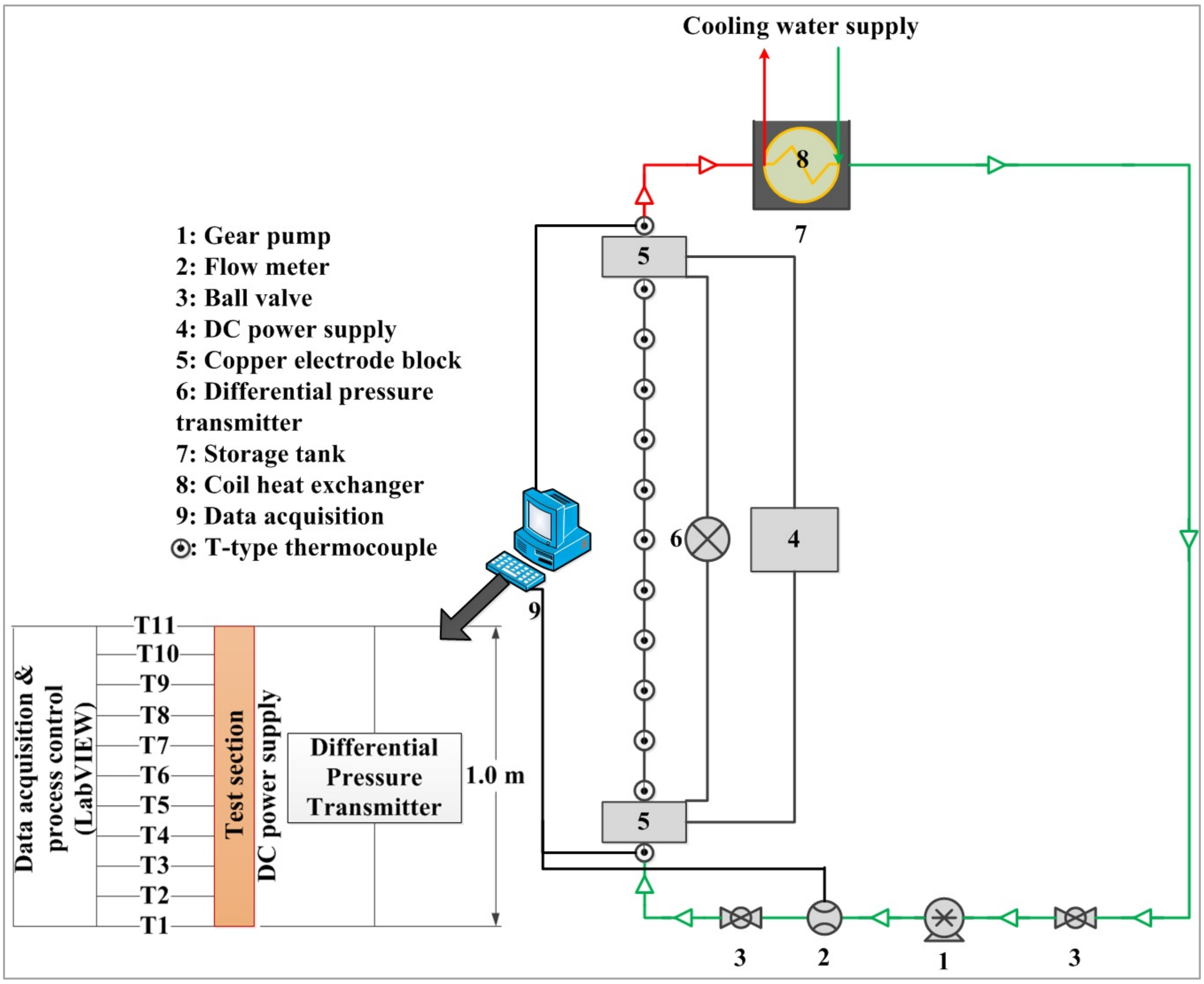

Fig. 1. A schematic representation of the closed loop experimental set-up.

The pressure drop across the test section was measured using a high precision differential pressure transmitter (Rosemount® 3051CD) with a reference accuracy of 0.004% of span, which was calibrated from 0 to 30 kPa. The pressure transmitter was attached to the inlet and outlet of the test section as shown in Fig. 1.

A coil heat exchanger was used to cool down the working fluid. Two stainless steel Swagelok ball valves were used to collect the working fluids after each run, and they permit the system to be cleaned and flushed easily. The volume of the experimental setup as well as the storage tank were kept to a minimum to minimise the nanofluids requirement because of its high price and long preparation time.

The thermocouples, ultrasonic flow meter, pressure transmitter and power supply instruments were connected to a data acquisition system to carry out the measurement, and the data acquisition system was interfaced with a computer by using a NI PCI-6251 board. A NI 9214 16-channel high-accuracy thermocouple module (National Instrument, UK) was employed for the measurement of temperature at high accuracy. 'Labview' software was used for the experimental system configuration as well as control.

It is very important to reach steady state conditions before taking the first data point, thus, the experimental rig was allowed to operate for at least one hour at the beginning of each run. This was necessary due to the thermal inertia of the system being fairly slow initially. Steady state conditions were said to be achieved when no significant variations in the mass flow rate, temperature, and pressure drop were observed. Once the experimental system achieved steady state conditions, data acquisition at the desired mass flow rate was easier as fluctuations in the system had subsided. It was very difficult to achieve the steady state conditions in the transitional regime because of the continuous variation in pressure, mass flow rate and temperature of the working fluid. But, the results were recorded as soon as the variation in the data was repeated periodically. The experiments were conducted from larger to smaller mass flow rate to minimise the stored residual heat in the insulation, which may have an effect on the following data point. Each of the data points was the average of 300 readings, which was captured by using the data acquisition system.

The Al_2O_3/DI-water and CuO/DI-water nanofluids were prepared using the two-step preparation method. In this study, an anionic surfactant, sodium dodecylbenzene sulfonate (SDBS), was used to stabilise the nanofluids with 0.10% and 0.15% weight fractions for Al_2O_3/DI-water and CuO/DI-water nanofluids, accordingly. Because, we have characterised Al_2O_3/DI-water and CuO/DI-water nanofluids with various weight concentrations of surfactant

[30]; and concluded that 0.10 wt% and 0.15 wt% of SDBS were the optimum amount of surfactant for Al_2O_3 and CuO nanofluids. The prepared nanofluids were found to be very stable, and did not show any visual signs of sedimentation for more than one week. The experiments were carried out over a few days and repeated three times, each of the data points was the average of three experimental runs. The properties of Al_2O_3 and CuO nanoparticles, and DI-water are shown in Table 2.

Table 2 Properties of DI-water and nanoparticles at $T = 300K$ [39].

Thermophysical properties	DI-water	Al_2O_3	CuO
Density, $\rho(kg/m^3)$	998.2	3700*	6400*
Specific heat, $c_p\ (J/kg.K)$	4182	765	535.6
Viscosity, $\mu(Ns/m^2)$	0.001		
Thermal conductivity, $k\,(W/m.K)$	0.60		

*Given by the supplier

2.2. Experimental data analysis

In this study, Al_2O_3/DI-water and CuO/water nanofluids with 0.20% to 0.50% of particle weight concentrations, and a tubular shape test section are used. It is assumed that the nanofluids flow across the test section are fully developed both hydrodynamically and thermally. From Eqs. (9) to (11), the parameters are calculated by applying a bulk temperature to simplify this analysis is one of the main assumptions. Moreover, the thermophysical properties (except thermal conductivity) of nanofluids were considered at a constant temperature of 300 K. The nanofluids thermophysical properties, such as density, thermal conductivity and specific heat, and viscosity have been calculated by applying Eqs. (1) to (4) [31].

Density of nanofluids,

$$\rho_{nf} = (1-\varphi)\rho_{bf} + \varphi\rho_{np} \tag{1}$$

The Eq. (1) is based on the concepts of mixing theory for ideal gas mixtures, and classical and statistical mechanisms.

Thermal conductivity of nanofluids,

$$\frac{k_{nf}-k_{bf}}{k_{bf}}=3.761088\varphi+0.017924(T-273.15)-0.30734 \tag{2}$$

Nanofluids' specific heat,

$$c_{p,nf}=\frac{(1-\varphi)(\rho c_p)_{bf}+\varphi(\rho c_p)_{np}}{\rho_{nf}} \tag{3}$$

Viscosity of nanofluids,

$$\mu_{nf}=(1+2.5\varphi)\times\mu_{bf} \tag{4}$$

The local convective heat transfer coefficient (h_x) was calculated using the following expression [40];

$$h_x=\frac{q''}{(T_{w,i}-T_b)_x} \tag{5}$$

where, q'' is the heat flux based on thermal power, L and D_i are the length and inner diameter of the test section, accordingly. $T_{w,i}$ and T_b are the inner wall and bulk temperatures of the test section, respectively at the axial location.

The Fourier's law of thermal conduction is expressed as $Q=-kA\frac{dT}{dD}$ or, $\int_{Di}^{Do}Q\frac{1}{dD}=-kA\int_{T_{w,i}}^{T_{w,o}}dT$. The inside wall temperature (as shown in Eq. 6) was calculated based on the analytical solution of the conduction equation, which involves the measured external wall temperature of the test section as the boundary condition and the thermal resistance (temperature dependent) of stainless steel.

$$T_{w,i} = T_{w,o} - \frac{Q}{2\pi k_w L}\left[\frac{D_o^2}{\left(D_o^2 - D_i^2\right)}\log\left(\frac{D_o}{D_i} - 0.5\right)\right] \tag{6}$$

In Eq. (6), Q represents the thermal power derived from bulk outlet and inlet temperature difference of the working fluid, D_o is the outer diameter, and k_w represents the thermal conductivity of stainless steel, and it is found from a linear curve fit of data found in the ASM Handbook [41], the resulting linear fit for k_w as a function of temperature is given by the following function,

$$k_w(T) = 0.0127 \times T + 13.23188 \tag{7}$$

The fluid local bulk temperature is interpolated using the Eq. (8) as,

$$T_b(x) = \frac{q'' S}{\dot{m} c_p} x + T_{b,in} \tag{8}$$

where, S is the surface perimeter ($S = \pi D_i$ for a circular tube), $\dot{m}$ is the mass flow rate, c_p is the specific heat, x represents the axial distance from the entrance of the test section, and the fluid bulk inlet temperature is $T_{b,in}$.

Then, the local Nusselt number was evaluated by using the local convective heat transfer coefficient (h_x),

$$Nu_x = \frac{h_x D_i}{k_x} \tag{9}$$

The dimensionless Reynolds number and Prandtl number can be estimated by using Eqs. (10) and (11),

$$\text{Reynolds number, } \mathrm{Re} = \frac{4\dot{m}}{\pi \mu D_i} \tag{10}$$

$$Mass\ flow\ rate\ (\dot{m}) = volume\ flow\ rate \times density$$

$$\text{Prandtl number, } \Pr = \frac{c_p \mu}{k} \tag{11}$$

The value of pressure drop was required to estimate the Darcy-Weisbach friction factor:

$$f = \frac{2\,\Delta P.D_i}{L.\rho.v^2} \tag{12}$$

Then Eq. (12) was modified to;

$$f = \frac{\Delta P.\rho.\pi^2.D_i^5}{8\,L.\dot{m}^2} \tag{13}$$

The pressure drop was found from the measurement of the differential pressure transmitter.

The required pumping power (P_p) of the fluid through the test section was calculated with Eq. (14).

$$P_p = \frac{\dot{m}}{\rho}\Delta P \tag{14}$$

The energy efficiency (η) for various weight concentration of nanofluids is the ratio of output heat transfer (Q) over the devoted thermal power (q'') [42]. This is shown in Eq. (15);

$$\eta = \frac{Q}{q''} \tag{15}$$

Exergy loss refers to irreversible losses that occur outside the control volume. It is a loss in work availability. In contrast, exergy destruction refers to irreversible losses within the control volume [43]. Exergy losses can be minimised by reducing the temperature difference of heat transport [44]. The rate of exergy loss is calculated by assuming there is no work or heat transfer between the system and surroundings. Exergy loss for a steady state nanofluid cooling system can be expressed by Eq. (16),

$$E_{loss} = T_e\left[C\ln\left(\frac{T_{out}}{T_{in}}\right)\right] \tag{16}$$

Exergy loss caused by a reduction in fluid pressure can be neglected for liquids, because they are incompressible [45]. The environmental temperature (T_e) is assumed to be the same as the fluids' inlet temperature. The heat capacity rate (C) can be calculated by using Eq (17).

$$C = c_p \, \dot{m} \tag{17}$$

2.3. Uncertainty

The maximum possible error for the variables and parameters associated in this study are calculated using the Kline and McClintock method [46], which can be expressed as follows;

$$U_R = \left[\left(\frac{\partial R}{\partial X_1} U_1 \right)^2 + \left(\frac{\partial R}{\partial X_2} U_2 \right)^2 + \ldots\ldots + \left(\frac{\partial R}{\partial X_n} U_n \right)^2 \right]^{0.5} \tag{18}$$

when, U_R is the uncertainty of the parameter $R,$ and R is a function of the independent variables X_1, X_2, …., X_n with the certainty of U_1, U_2, …., U_n.

Table 3 shows the vales of uncertainties from different instruments, and the uncertainties of experimental parameters are summarised in Table 4.

Table 3. Uncertainties of instruments

Variable	Uncertainty (%)
Wall temperature, $T_{w,i}$	0.435
Bulk temperature, T_b	0.627
Load regulation	0.5
Differential pressure transmitter	0.004
Ultrasonic flow meter	3%

Table 4. Uncertainties of experimental parameters and variables

Variable	Uncertainty error (%)
Heat transfer coefficient	0.50
Pumping power	5
Exergy loss	6

2.4. Validation

In this study, the Nusselt number and friction factor were validated in the laminar, transitional, and turbulent flow regions by comparing the results with published data points. The results for DI-water was utilised to validate the experimental set up, because there are no other results or data points available in the existing literature for Al_2O_3/DI-water and CuO/DI-water nanofluids at the same experimental conditions.

2.4.1. Nusselt number

Ghajar and Tam [25] proposed correlations for Nusselt number in the laminar and turbulent flow regimes;

$$Nu_{lam} = 1.24\left[\left(\mathrm{Re}\,\mathrm{Pr}\,\frac{D_i}{x}\right) + 0.025\,(Gr\,\mathrm{Pr})^{0.75}\right]^{\frac{1}{3}}\left(\frac{\mu_b}{\mu_w}\right)^{0.14} \tag{19}$$

$$\text{Local bulk Grashof number, } Gr = \frac{g\beta\rho^2 D_i^3 (T_{wi} - T_b)}{\mu^2} \tag{20}$$

$$Nu_{turb} = 0.023\,\mathrm{Re}^{0.8}\,\mathrm{Pr}^{0.385}\left(\frac{x}{D_i}\right)^{-0.0054}\left(\frac{\mu_b}{\mu_w}\right)^{0.14} \tag{21}$$

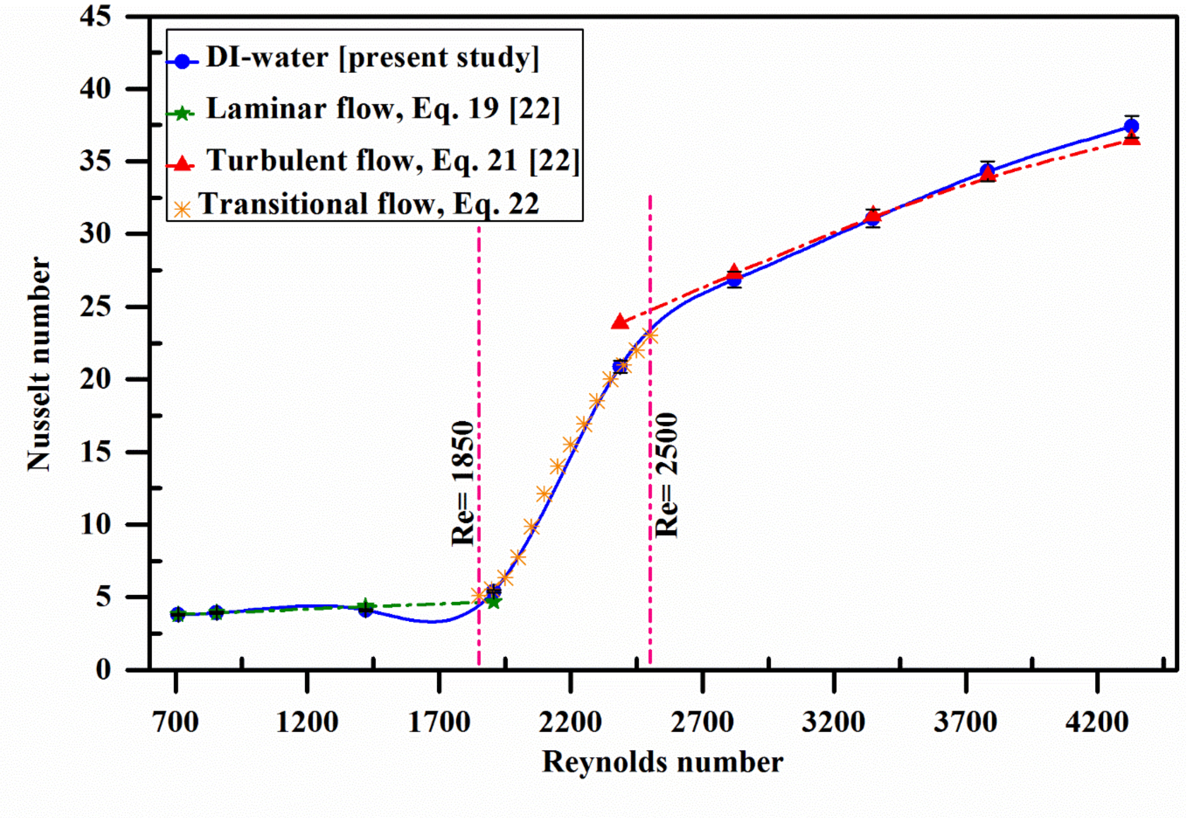

Fig. 2. Nusselts number vs. Reynolds number results compared with the correlations introduced by Ghajar and Tam [25] for DI-water at x/D = 21.88.

Ghajar and Tam [25] formulated an equation for the transitional flow, and in this study, it was modified for a developing length inlet condition;

$$Nu_{trans} = Nu_{lam} + \left[e^{\frac{\mathrm{Re}_{trans} - \mathrm{Re}}{65}} + Nu_{turb}^{-0.935} \right]^{-0.935} \tag{22}$$

Fig. 2 shows that, the Nusselt number vs Reynolds number results have good agreements among the equations developed by Ghajar and Tam [25] with the allowable dissimilarity approximately 1.90%, 2.62% and 2.1% in the laminar, turbulent and transitional flow regimes, respectively, on average. This type of validation technique improves the confidence level in the measurement as well as the data reduction methodology.

2.4.2. Friction factor

Fig. 3 shows the friction factor versus Reynolds number results for DI-water compared with the Blasius equation ($f = 0.3164\,\mathrm{Re}^{-0.25}$), the Poiseuille equation ($f = \frac{64}{\mathrm{Re}}$), and the modified Blasius equation developed by Allen and Eckert [47]. They proposed that a viscosity correction factor, $\left(\frac{\mu_b}{\mu_w}\right)^{-0.25}$, needs to be multiplied by the Blasius equation.

From Fig. 3, when considering the transitional flow regime, it starts at a Reynolds number of approximately 1850. The shift from the transitional to turbulent flow regime begins at a Reynolds number of roughly 2500, instead of the conventional Reynolds number value of 2300. The late transition occurs due to the effect of the inlet of the test section as described by Meyer and Olivier [29].

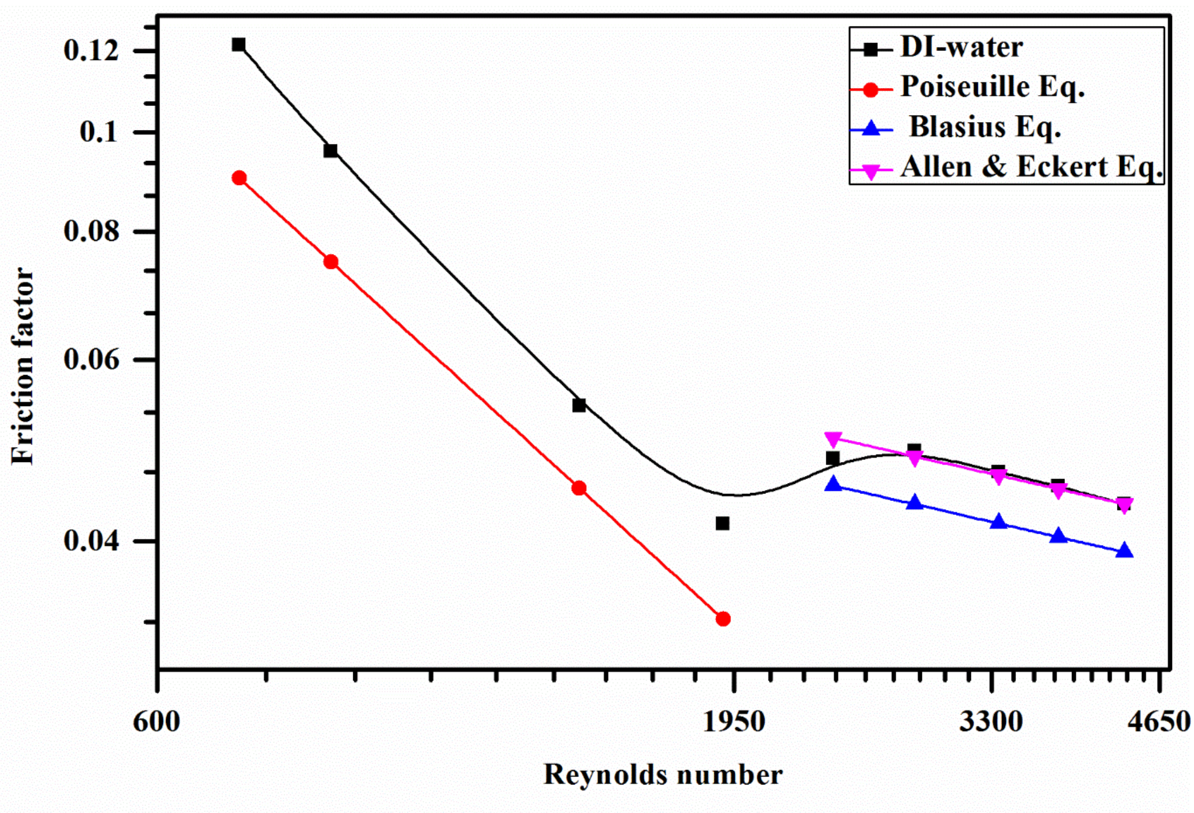

Fig. 3. Friction factors of DI-water as a function of the Reynolds number.

For the turbulent data, the results using the Allen and Eckert [47] equation correlate fairly well with the experimental DI-water result with an average variation around 0.44%. The friction factor of the Blasius correlation was observed to be about 9% lower than the value of experimental result for DI-water. In the laminar flow region, around 20% dissimilarity was found between the experimental and predicted (calculated by using Poiseuille equation) friction factors. This may be because of the effect of secondary flow, which is capable of enhancing the friction factor, particularly in a test section under constant and uniform heat flux boundary conditions [48]. Tam and Ghajar [48] suggested that the friction factor in the laminar flow regime increases with the increment of the overall heat flux. For this reason, there was a difference between wall and bulk coolant temperature across the length of the test section [49].

3. Results and discussion

The local convective heat transfer coefficient as a function of axial distance along the test section for Al_2O_3/DI-water and CuO/DI-water nanofluids are presented in Figs. 4 and 5 respectively, with nanoparticle weight fractions 0.20 wt%, 0.30 wt% and 0.50 wt% in both the laminar and turbulent flow regimes.

Under laminar flow, *Re* = 1400 (i.e. Fig. 4a and 5a), the local convective heat transfer coefficient of both nanofluids showed a significant enhancement in comparison to DI-water. The heat transfer coefficient is directly proportional to k/δ_t (where, δ_t = thermal boundary layer thickness). Therefore, an enhancement to the convective heat transfer coefficient may be attributed to the increase of thermal conductivity as well as the delaying and disturbance of thermal boundary layers. Previous studies have demonstrated the reasons for the improvement in heat transfer of nanofluids, which include mixing effects of nanoparticles near the tube wall, thermal conductivity enhancement, Brownian motion of particles, particle shape, size and migration, reduction of boundary layer thickness, and delay in the development of the boundary layer [26, 50].

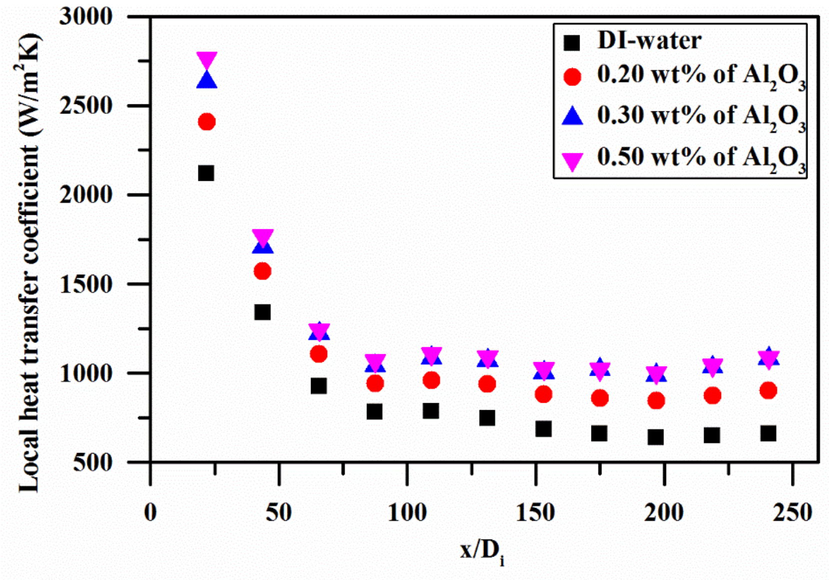

(a)

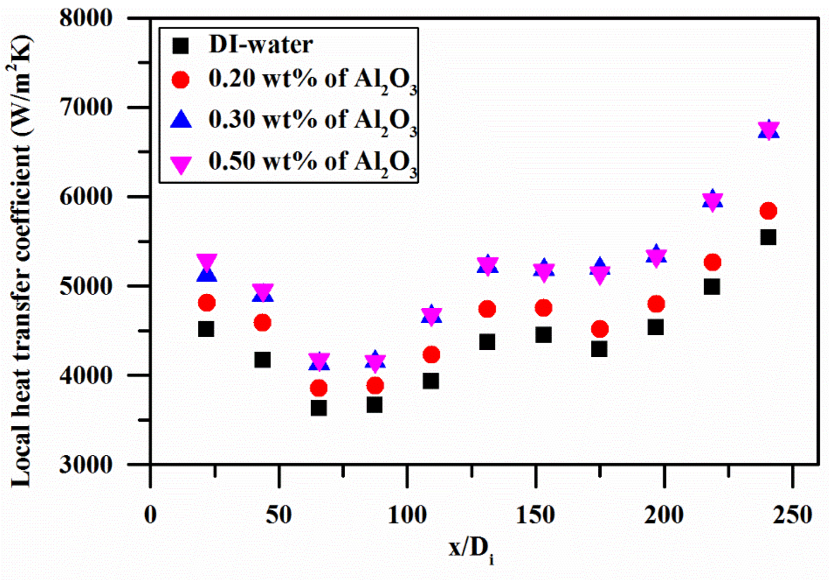

(b)

Fig. 4. Local convective heat transfer coefficient of Al_2O_3/DI-water nanofluids along with axial position. (a) Laminar flow (*Re*=1400); (b) turbulent flow (*Re*=2800).

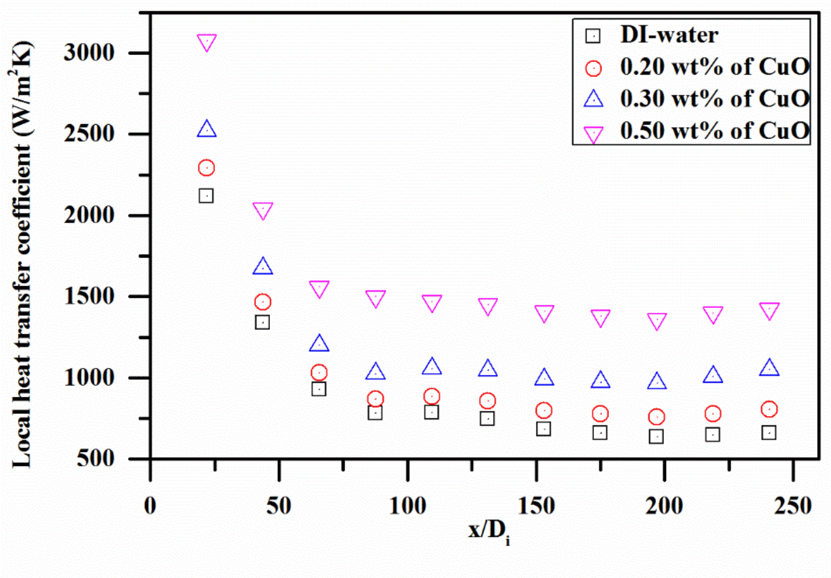

(a)

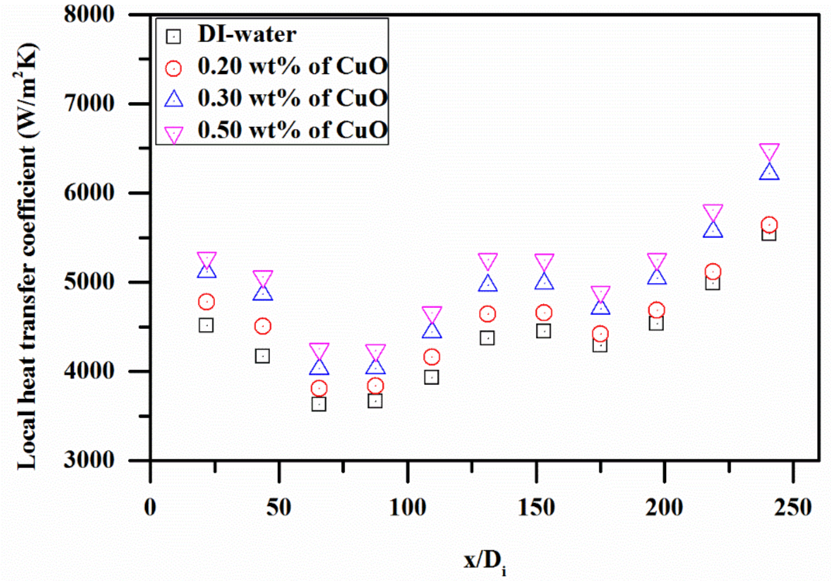

(b)

Fig. 5. Local convective heat transfer coefficient of CuO/DI-water nanofluids along with axial position. (a) Laminar flow (*Re*=1400); (b) turbulent flow (*Re*=2800).

From the Figs. 4a and 5a, a higher value for the heat transfer coefficient was noticed at the entrance of the experimental test section. This is because, the thickness of the thermal boundary layer is zero at the beginning, which leads the heat transfer coefficient to infinity. Because, the thermal boundary layer may be affected by the chaotic movement as well as Brownian motion of the nanoparticles [51]. The thickness of the thermal boundary layer rises with the progression along the axial distance until both the thermal boundary layer thickness and heat transfer coefficient are constant. Therefore, thermal conductivity enhancement, reduction in the thermal boundary layer or both are the possible reasons for the improvement in the heat transfer coefficient observed for the nanofluids. In addition, the Eq. (19) shows that the Nusselt number is inversely proportional with the axial position of the test section, which also confirm the observation of enhancement in the heat transfer coefficient with the decrement of axial position in laminar flow regime.

The local convective heat transfer coefficient of Al_2O_3/DI-water and CuO/DI-water nanofluids under turbulent conditions, i.e. *Re*= 2800, are illustrated in Figs. 4b and 5b. The convective heat transfer coefficient increases with the progression along the axial positon of the test section, which is on the contrary to the trend observed under laminar flow. Two different data trends were reported for the laminar and turbulent flow regimes, because two different mechanisms are apparent for heat transfer improvement in the two flow regimes [18]. The thermal entry length is defined as $x_{fd,t} \approx 0.05 \mathrm{Re}_D \Pr D_i$ and $x_{fd,t} \approx 10 D_i$ for laminar flow and turbulent flow condition, respectively [18]. Hence, there was a development in the thermal boundary layer across all the axial positions under laminar flow, whereas, this development was more than 10 times of its axial length for turbulent flow regime. Furthermore, the Eq. (21) shows a proportional relationship between Nusselt number and axial positon of the test section, which also support the trends shown in Figs. 4b and 5b.

As mentioned earlier in this section, the increase in the thermal conductivity and/or a decrease in thermal boundary layer thickness helps to enhance the heat transfer performance of the system, however, a rise in viscosity contributes to increasing the boundary layer thickness, which may result in a reduction in heat transfer performance [52]. Therefore, comparing the heat transfer of nanofluids with the base fluid by varying the Reynolds number is usually a best basis of comparison, because, the viscosity value of the nanofluid is larger than that of its base fluid [10]. Such a comparison is shown in Fig. 6.

The results show that, the maximum enhancement in heat transfer coefficient of the 0.50 wt% Al_2O_3/DI-water nanofluid was 11%, and the enhancement was 25% for the 0.50 wt% CuO/DI-water nanofluid.

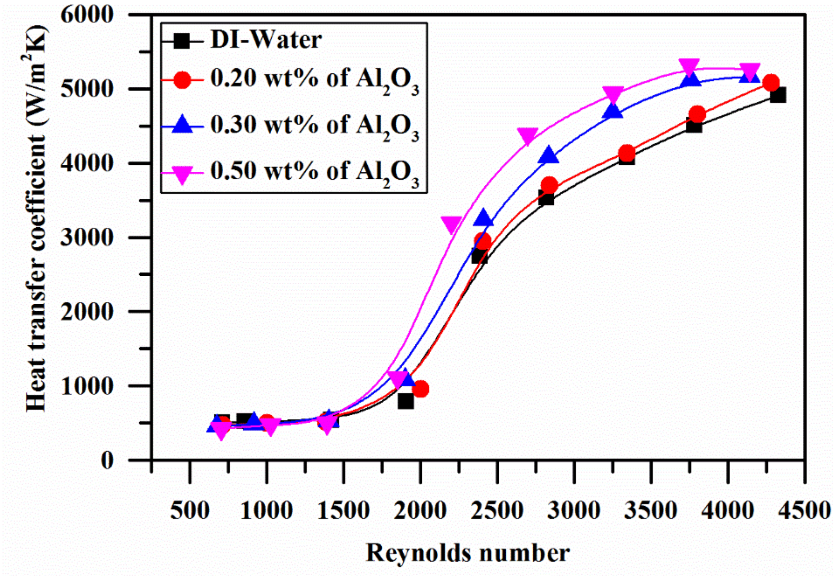

(a)

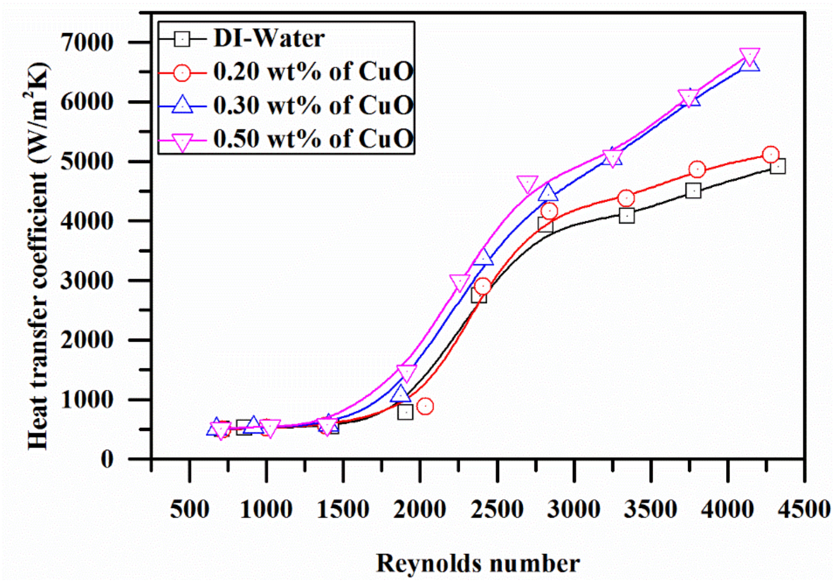

(b)

Fig. 6. Convective heat transfer coefficient as a function of Reynolds number (a) Al_2O_3/DI-water, and (b) CuO/DI-water nanofluids at $x/D_i = 110$.

Under laminar flow conditions, the heat transfer coefficients for all fluids (DI-water and both of the nanofluids with every weight fraction of nanoparticles) were almost same. This may be attributed to the fact that the nanofluids exhibit shear thinning behaviour at low shear rates [30], which increases the viscosity and hence, reduces the value of heat transfer coefficient of the nanofluids.

When considering the transitional flow regime, the greater weight fraction nanofluids exhibited earlier transition in comparison to lower weight fraction nanofluids. This is because, higher weight fraction nanofluids have a larger value of viscosity, hence, the results shifted [21]. The aluminium oxide and copper oxide nanofluids demonstrate converging and diverging trends at the higher weight concentrations and Reynolds number, accordingly. This may be associated with non-linear rheological behaviour of those nanofluids, and the attainment of shear thickening behaviour at different shear rates [30].

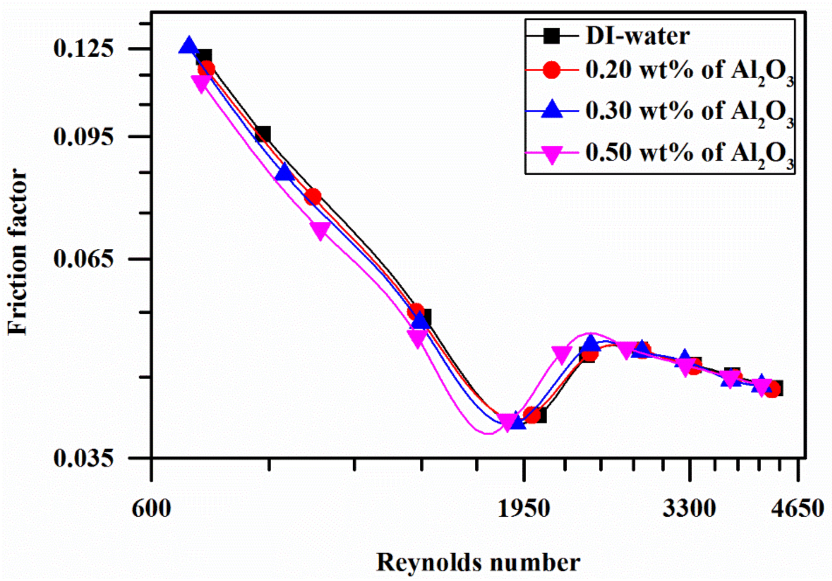

(a)

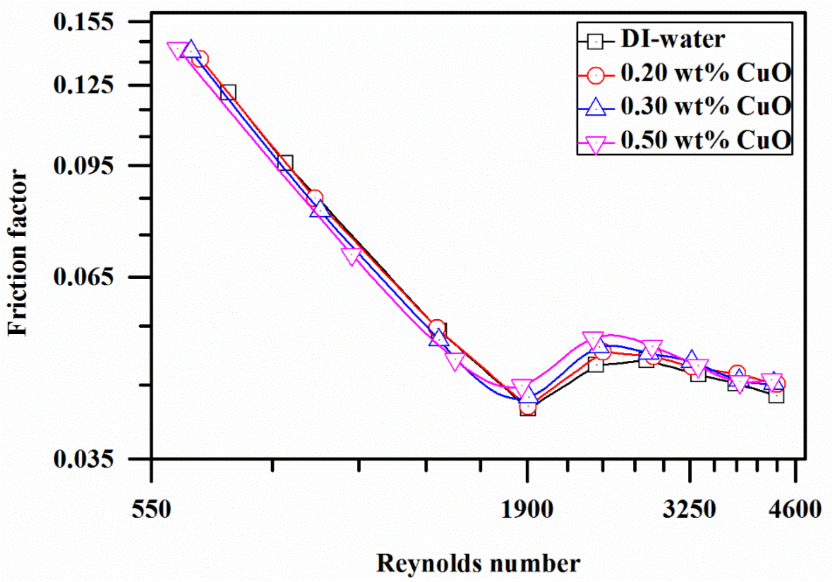

(b)

Fig. 7. Friction factor as a function of Reynolds number (a) Al_2O_3/DI-water, and (b) CuO/DI-water nanofluids.

Fig. 7 demonstrates the friction factors of DI-water, Al_2O_3/DI-water and CuO/DI-water nanofluids at different weight concentrations as a function of Reynolds number for the entire flow range. The maximum changeable friction factor value with respect to DI-water were for 0.50 wt% Al_2O_3/DI-water and CuO/DI-water nanofluids. In the laminar regime, the average friction factor for the 0.50 wt% Al_2O_3/DI-water and CuO/DI-water nanofluids were found to be 10% and 2.9% lower than the friction factor of DI-water respectively. In the turbulent flow regime, the average enhancement of the friction factor for both Al_2O_3/DI-water and CuO/DI-water nanofluids with 0.50 wt% of nanoparticles were approximate 0.4% and 3.5%, respectively when compared to DI-water. The friction factors of the 0.20 wt% Al_2O_3/DI-water and CuO/DI-water nanofluids were very similar to the friction factor of DI-water; this is most likely due to the low weight concentration of nanoparticles in the base fluid.

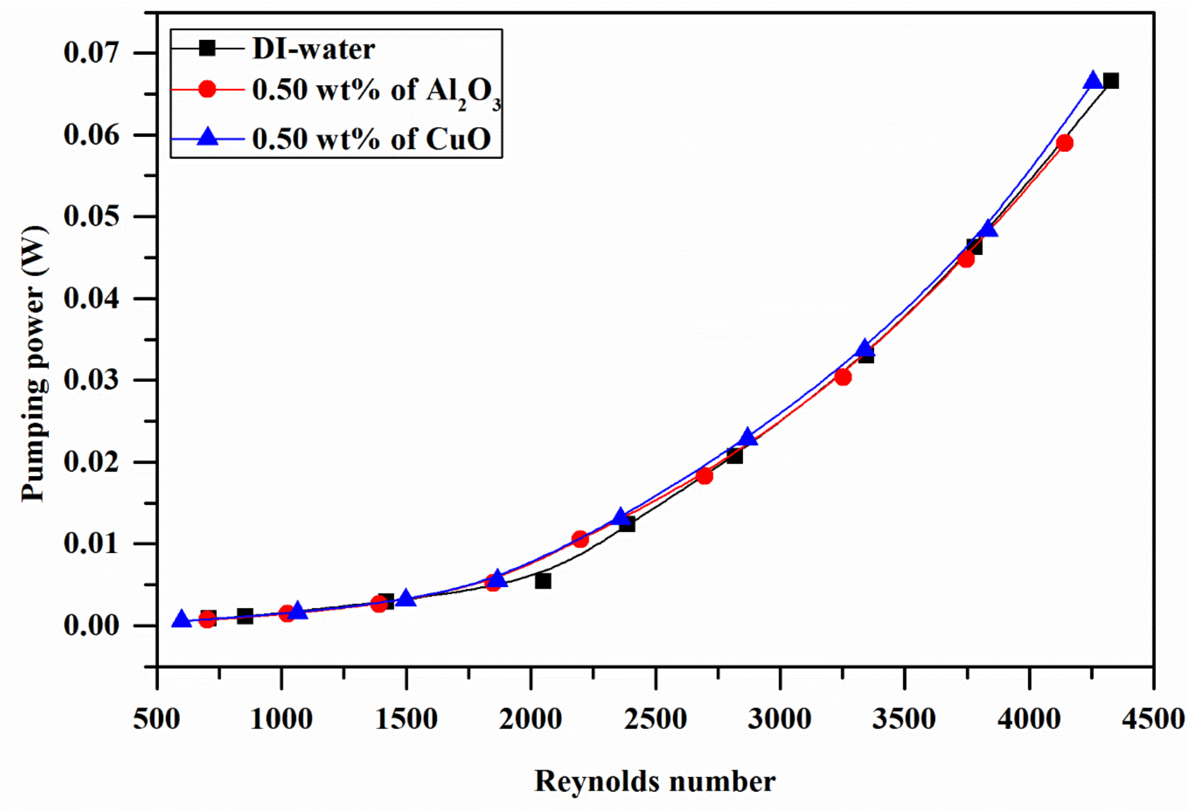

Fig. 8. Pumping power versus Reynolds number for DI-water, Al_2O_3/DI-water and CuO/DI-water nanofluids with highest weight concentration of nanoparticle.

Fig. 8 shows the enhancement of pumping power as a function of Reynolds number. The pumping power was similar for both of the nanofluids and DI-water at the low Reynolds number, $Re < 1800$. As the Reynolds number increased above 1800, the pumping power of the nanofluids began to increase. Therefore, pumping power becomes more significant for higher mass flow rates, and as a result, it may influence the exergetic performance of the nanofluids [53].

Pumping power is a function of the mass flow rate, density, and pressure drop (Eq. 14). Increases in pressure drop during the flow of the working fluid is an important parameter in determining the efficiency of nanofluids applications as the pressure drop and pumping power of the working fluid are closely related. There are a few properties which could influence pressure drop such as density and viscosity. It is expected that the pressure drop may increase with enhancements of the density and viscosity of the working fluid. This is one of the disadvantages for nanofluids applications as a cooling liquid.

From the Fig. 8, the average pumping power enhancement for CuO/DI-water nanofluids was 3.9% with respect to DI-water in the transitional and turbulent flow regimes. In the case of Al_2O_3/DI-water nanofluids, there was a slight decrease in the pumping power in comparison to DI-water. This may be attributed to the difference in viscosity and density of the Al_2O_3/DI-water nanofluids. Hence, it was concluded that, Al_2O_3/DI-water and CuO/DI-water nanofluids with a nanoparticle concentration of 0.5 wt% exhibit optimal heat transfer performance, with reasonable pumping power consumption.

Fig. 9 shows the effective trend of energy efficiency as a function of the nanoparticle weight fraction as well as the input power. The energy efficiency rises significantly as the nanoparticle weight fraction and input power increases. The maximum energy efficiency was found for 0.50 wt% CuO/DI-water nanofluids at around 84% with 284 W input power, which was approximately 11.4% higher than the average energy efficiency of DI-water. The enhancement of energy efficiency of the 0.50 wt% Al_2O_3/DI-water nanofluid was 6.1% higher than DI-water.

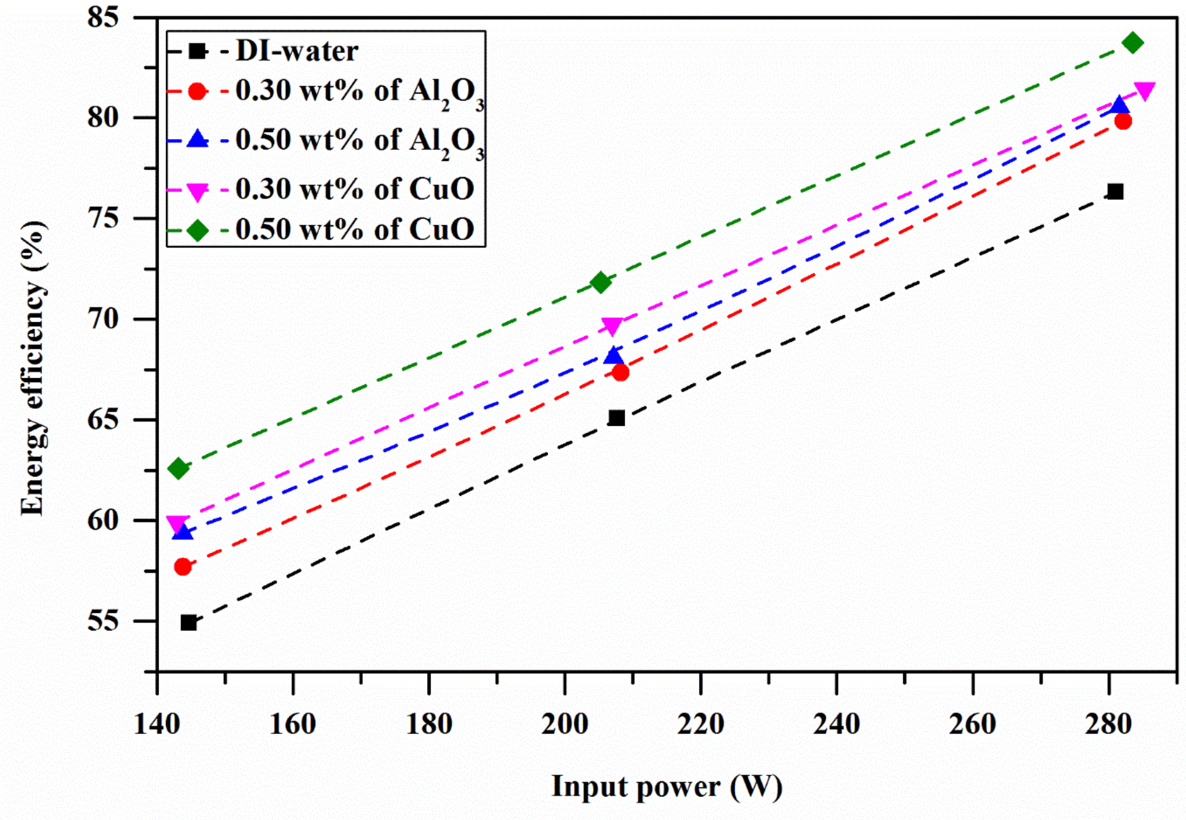

Fig. 9. Energy efficiency of nanofluids and DI-water with input power at different nanoparticle weight fractions.

In this study, the maximum input power employed was 285 W, for input powers greater than this magnitude the phenomenon known as the geyser effect may occur [54], which may decrease the thermal efficiency of nanofluids. The enhancement in the energy efficiency for both of the nanofluids was attributed to the effect of Brownian motion of the nanoparticle in the base fluid, which improves the heat transfer between the fluid and the tube wall. Brownian motion is an important feature which is utilised for micro-convection. It is apparent when the size of the particles in a system is very small, hence, Brownian motion decreases, as the size of the particle increases [55, 56]. However, Brownian motion is a result of the continuous collisions between nanoparticle and nanofluid molecules, causing chaotic motion. With an increase in the chaotic motion, this phenomenon may introduce an energy exchange throughout the wall of the test section, and hence, the magnitude of heat transfer between the fluid and tube wall increased considerably, leading to an enhancement of the energy efficiency.

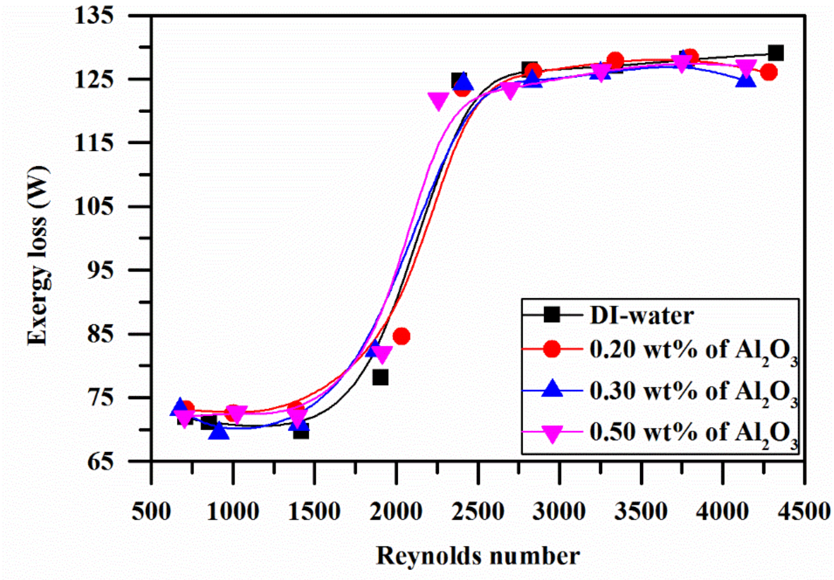

(a)

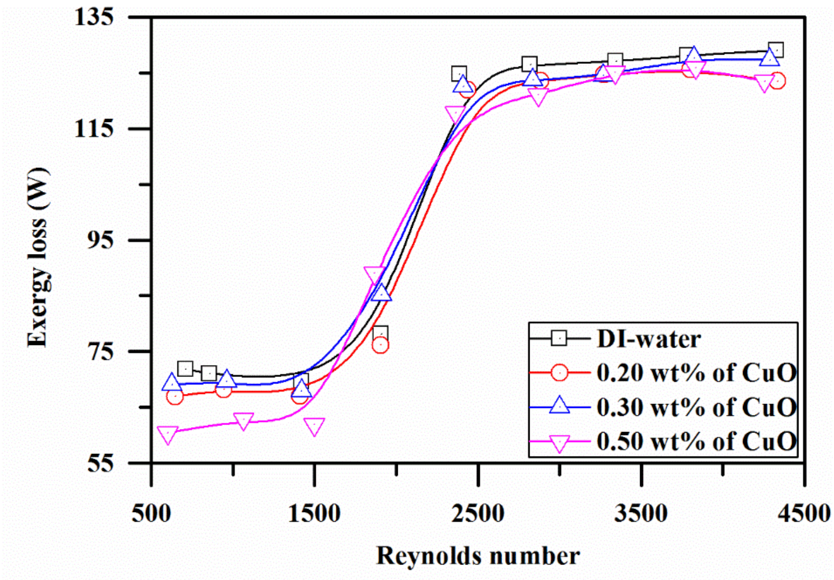

(b)

Fig. 10. Exergy loss versus Reynolds number with different weight fractions of nanoparticles (a) Al_2O_3/DI-water, and (b) CuO/DI-water nanofluids.

Fig. 10 illustrates the exergy loss variation with nanoparticle weight concentration for DI-water, Al_2O_3/DI-water and CuO/DI-water nanofluids. DI-water showed the highest exergy loss in comparison to the nanofluids for all weight fractions except the Al_2O_3/DI-water nanofluids in the laminar flow regime. The best exergetic utilisation of a thermal system is found when the entropy generation is a minimum [57]. At greater nanoparticle weight fractions, the entropy generation may decrease, and thus, comparatively an increase in exergy efficiency was observed for the nanofluids than DI-water. Furthermore, it can be noted that the addition of nanoparticles to the base fluid leads to an enhancement of the effective heat transfer surface area. Therefore, in this study, the exergy loss was calculated using the Eq. (16), which is a function of specific heat capacity, mass flow rate, as well as inlet and outlet temperature of the working fluid. The specific heat capacity decreases with the increasing weight fraction of nanoparticles. In addition, the mass flow rate increases with increasing weight fraction of nanoparticles, because, it is dependent on the density of the working fluid. The reduction in the specific heat capacity was more significant than the rise in mass flow rate of the nanofluids at greater weight concentrations; as a result, the exergy loss was a minimum at the highest weight fraction of nanoparticles. The above reasons may result in a reduction in the exergy loss while using nanofluids. This result is in agreement with Khairul et al [31]. They analysed the exergy loss of DI-water and CuO/DI-water nanofluids with three different volume concentrations of nanoparticles, and concluded that the exergy loss decreased for an increasing volume fraction of nanoparticles.

The experimental results were compared with the popular correlations proposed in various studies. The Sundar and Sharma [34], and Lienhard [35] classical correlations were considered for analysing the Nusselt number of Al_2O_3/DI-water and CuO/DI-water nanofluids in laminar flow regime. Moreover, the Duangthongsuk and Wongwises [36], Dittus and Boelter [37], and Vajjha and Das [38] proposed Nusselt number equations for turbulent flow were also applied to compare the experimental Nusselt number. The correlations are demonstrated below;

Sundar and Sharma [34]

$$Nu = 0.2624(\mathrm{Re}^{0.5860})(\mathrm{Pr}^{0.3})\,(0.001+\varphi)^{0.07094} \tag{23}$$

Lienhard [35]

$$Nu = 1.619(x^{+})^{-1/3} \tag{24}$$

Dimensionless distance, $x^{+} = \dfrac{2(x/D_i)}{\mathrm{Re}\,\mathrm{Pr}}$

Duangthongsuk and Wongwises [36]

$$Nu = 0.074(\mathrm{Re}^{0.707})(\mathrm{Pr}^{0.385})(\varphi^{0.074}) \tag{25}$$

Dittus and Boelter [37]

$$Nu = 0.023(\mathrm{Re}^{0.8})(\mathrm{Pr}^{0.3}) \tag{26}$$

Vajjha and Das [38]

$$Nu = 0.065(\mathrm{Re}^{0.65} - 60.22)(1 + 0.0169\varphi^{0.15})(\mathrm{Pr}^{0.542}) \tag{27}$$

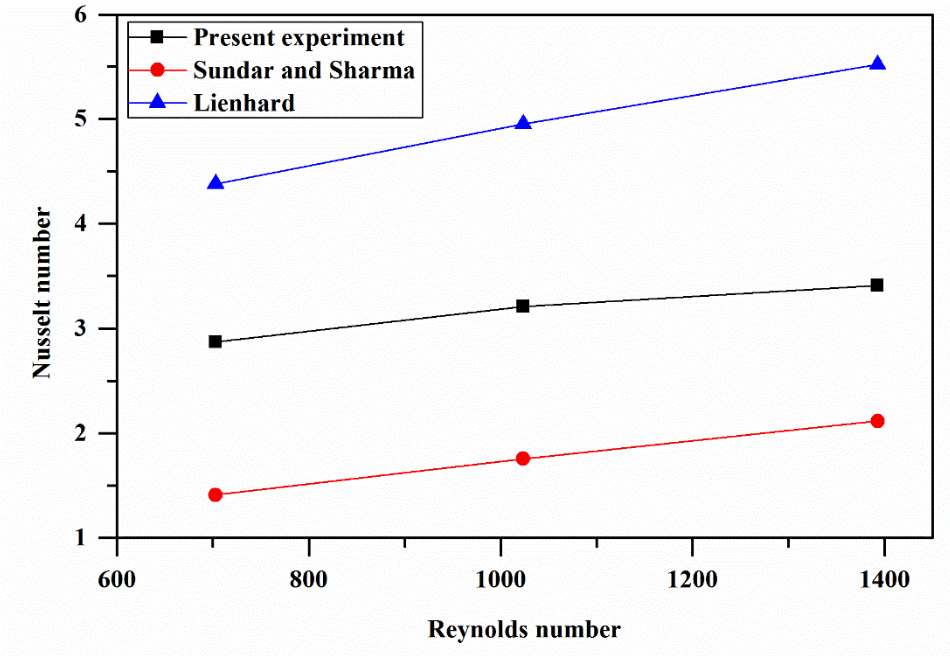

(a)

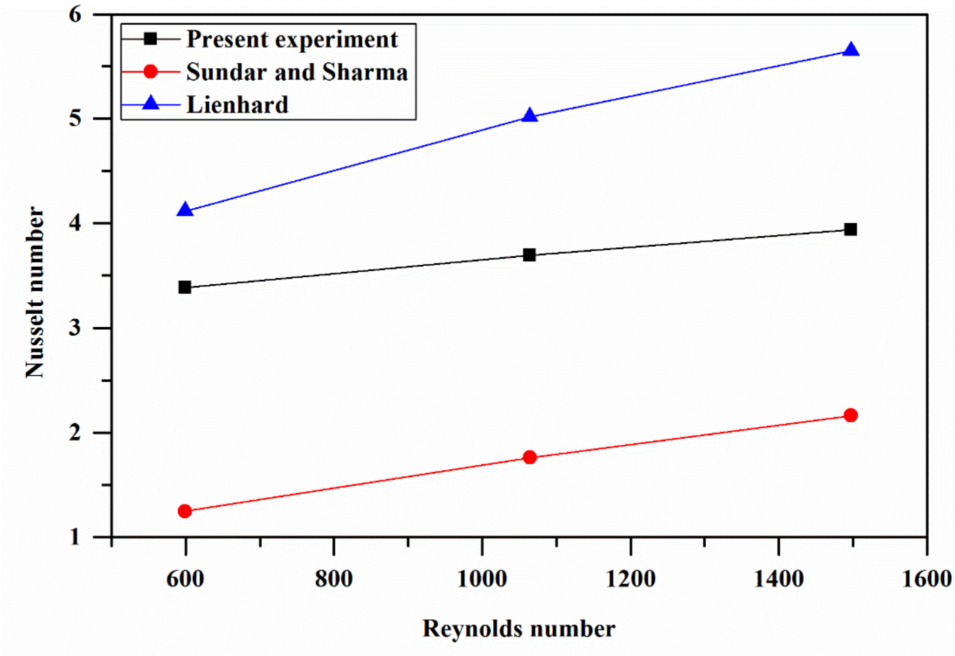

(b)

Fig. 11. Comparisons of experimental Nusselt number with proposed correlations at 0.50% wt% of nanoparticle for laminar flow (a) Al_2O_3/DI-water, and (b) CuO/DI-water nanofluids.

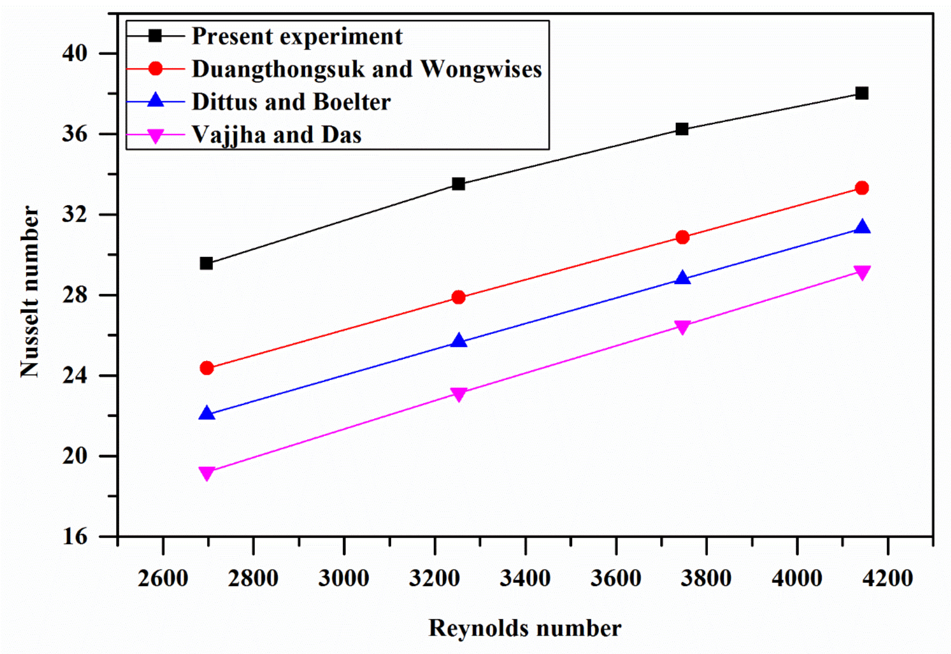

(a)

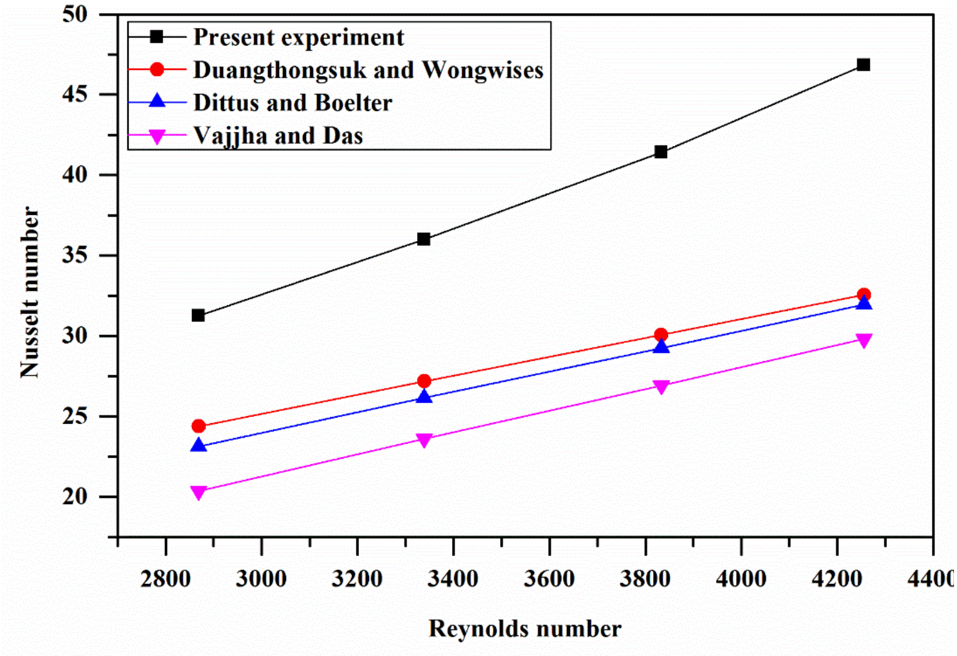

(b)

Fig. 12. Comparisons of experimental Nusselt number with proposed correlations at 0.50 wt% of nanoparticle for turbulent flow (a) Al_2O_3/DI-water, and (b) CuO/DI-water nanofluids.

The comparison between experimental Nusselt number and predicted Nusselt number (calculated from Eqs. 23-27) is demonstrated in Figs. 11 and 12 for laminar and turbulent flow regime with 0.50 wt% of nanoparticle. It is observed that the experimental Nusselt number of nanofluids was higher compared to the predicted Nusselt number. This may be associated with the different experimental assumptions; the current experimental considerations may not be the similar with other studies. In addition, SDBS was used in this analysis as a surfactant to stabilise the Al_2O_3 and CuO nanoparticles, which may enhance the heat transfer performance of nanofluids. However, some of the correlations (such as Dittus and Boelter) did not consider the impact of volume concertation of nanofluids on the Nusselt number.

Consequently, the following correlations are introduced to fulfil the gap between the values of experimental and predicted Nusselt number. The new Nusselt number correlations are a function of Reynolds number, Prandtl number and nanofluids' volume concentration.

For Al_2O_3/DI-water in laminar flow regime

$$Nu = 0.86(\mathrm{Re}^{0.205})(\mathrm{Pr}^{0.33})(\varphi^{0.1}) \tag{28}$$

For CuO/DI-water in laminar flow regime

$$Nu = 1.04(\mathrm{Re}^{0.205})(\mathrm{Pr}^{0.33})(\varphi^{0.1}) \tag{29}$$

For Al_2O_3/DI-water in turbulent flow regime

$$Nu = 0.033(\mathrm{Re}^{0.85})(\mathrm{Pr}^{0.385})(\varphi^{0.1}) \tag{30}$$

For CuO/DI-water in turbulent flow regime

$$Nu = 0.016(\mathrm{Re}^{0.957})(\mathrm{Pr}^{0.385})(\varphi^{0.1}) \tag{31}$$

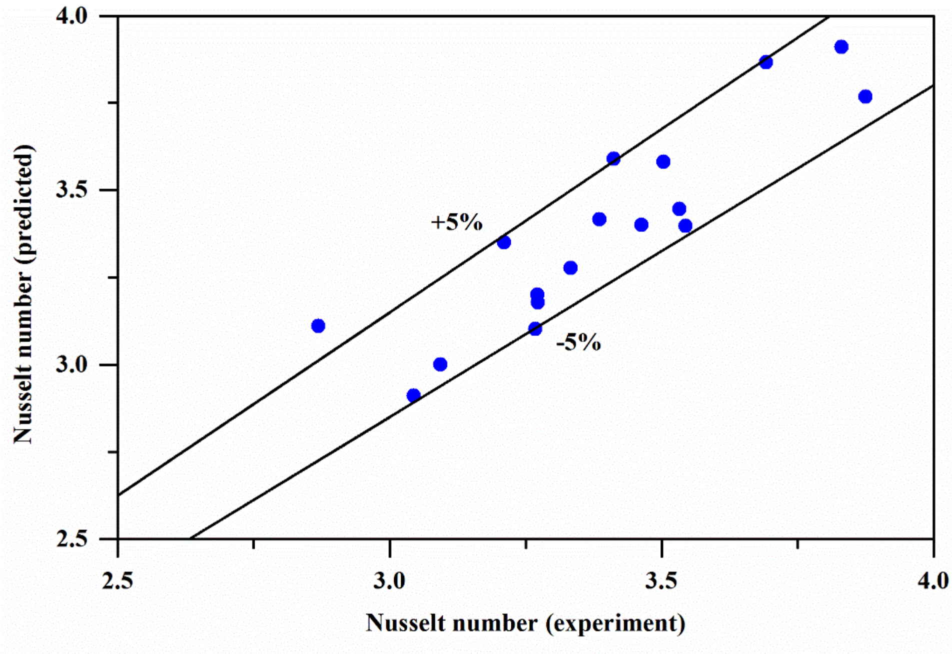

(a)

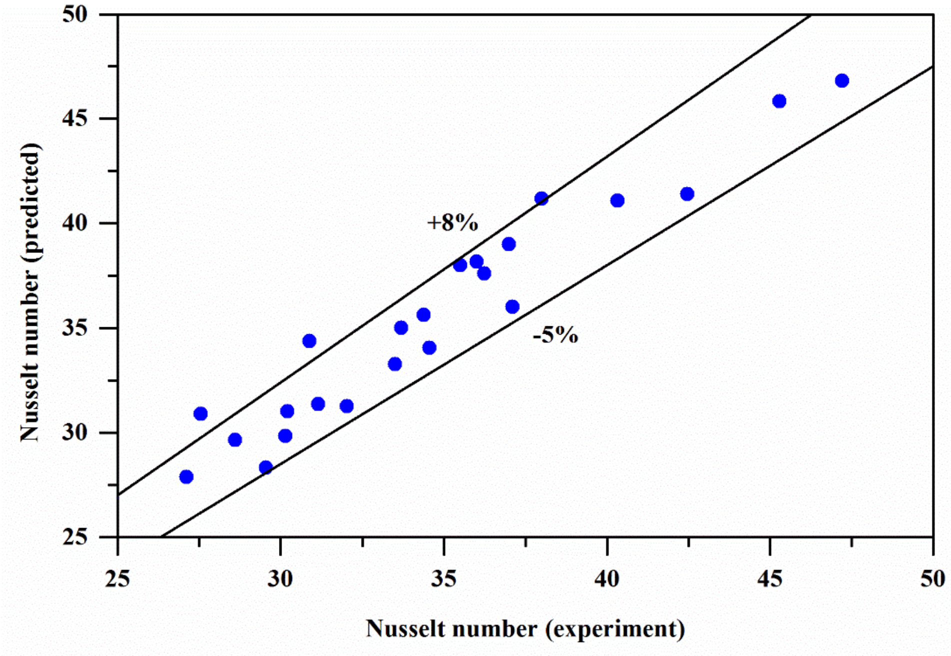

(b)

Fig. 13. Comparison of experimental and predicted Nusselt number of nanofluids based on the new correlation (a) laminar flow regime, (b) turbulent flow regime

The above developed correlations in Eqs. (28) to (31) are valid under the laminar and turbulent flow regimes for Al_2O_3/DI-water and CuO/DI-water nanofluids with the weight fractions from 0.20% to 0.50%. The Fig. 13 shows the variations of predicted Nusselt numbers (from Eqs. 28-31) versus experimental Nusselt numbers. For the laminar flow condition, the newly proposed correlations can predict the Nusselt number with a maximum deviation of +5% and -5% for all the weight concentrations of Al_2O_3 and CuO nanofluids, whereas, the maximum variation was found +8% and -5% for turbulent flow regime. There is a very good agreement between the values of experimental Nusselt number and the predicted Nusselt number from newly introduced equations. Therefore, the correlations proposed in this study may help to predict the heat transfer potential of aluminium oxide and copper oxide nanofluids in both laminar and turbulent flow conditions.

4. Conclusion

Al_2O_3/DI-water and CuO/DI-water nanofluids with three different nanoparticles weight concentrations were analysed in this study under laminar, transitional and early turbulent flow regimes. Both the Al_2O_3/DI-water and CuO/DI-water nanofluids showed a noticeable rise in heat transfer coefficient in comparison to the DI-water for all flow regimes (laminar, transitional and turbulent). Moreover, this study also involved the analyses of friction factor, pumping power, energy efficiency and exergy losses to determine the potential overall thermal performance of different classes of nanofluid in a smooth stainless steel tube with vertical orientation. Results showed that the friction factor was decreased as either the Reynolds number as well as weight fraction of nanoparticles in the nanofluids increased. Pumping power was also increased with the increment in nanoparticle weight concentrations due to higher viscosity. Although, there was a penalty associated with the pumping power for nanofluids, it was found that the energy efficiency of the nanofluids increased at higher nanoparticle weight concentrations and input power. The 0.50 wt% CuO/DI-water nanofluid showed the highest energy efficiency of about 84% at an input power of 284 W. Furthermore, new correlations were introduced to predict the Nusselt number of aluminium oxide and copper oxide nanofluids for laminar and turbulent flow regimes.

Based on the experimental observations in this study, it was concluded that CuO/DI-water nanofluids has the highest energy efficiency and heat transfer coefficient, as well as lowest friction factor and exergy loss. These characteristics make CuO/DI-water nanofluids an ideal and prominent candidate for heat transfer fluids in thermal applications.

Acknowledgements

The authors gratefully acknowledge the financial support provided by the University of Newcastle (Australia), Granite Power Pty Ltd and the Australian Research Council through the ARC-Linkage grant LP100200871, for the present study. The authors also would like to thank Dr Kalpit Shah for his valuable advice and supervision. The authors' sincerer thanks also go to Dr Priscilla Tremain for having patiently gone through the draft of this study and provided useful recommendations and suggestions, which significantly improved its presentation. The authors are thankful to Dr Ron Roberts for providing the technical supports and useful suggestions.

Appendix A.

Thermocouple calibration procedure

The T-type thermocouples (range: -200℃ to 350℃, uncertainty: 0.50℃) do not need to be calibrated in the technical sense as this is done by NI-instrumentation with the reference of NIST calibration curves. However, all of the thirteen thermocouples were tested to confirm that there was no connection or manufacturing flaws, which may involve erroneous readings. The thermocouples were immersed in a well-maintained temperature bath at three different temperatures, 41ºC, 58.5ºC, 91.5ºC, respectively. The results were the average of 300 data points, and shown in Table A1.

Table A1. Thermocouples testing result.

Avg. temperature (℃)	Min. temperature (℃)	Max. temperature (℃)	Standard deviation (℃)
40.91	40.71	41.16	0.12
58.54	58.06	58.97	0.27
91.77	90.94	92.63	0.50

It can be observed that the standard deviations are below or equal to the recommended uncertainty of the T-type thermocouples.

Appendix B.

Differential pressure transmitter calibration procedure

Regular calibration of the differential pressure transmitter was performed to ensure accurate pressure measurements. Firstly, a pressure transmitter as well as a digital calibration pressure gauge (accuracy: 0.05% FS, range: 0 to 103.4 kPa, Michigan, USA) were connected to a Dwyer low pressure calibration pump (output range: -40 to 40 kPa, Michigan, USA) with an adjusting resolution up to 0.01 Pa. Later, the pressure in the pressure pump was gradually increased for a range of pressure readings from 0 to 30 kPa. The pressure was recorded using a LabVIEW program, which output the reading of the pressure drop of the transmitter. Then, the value was compared with the reading of Dwyer digital calibration pressure gauge.

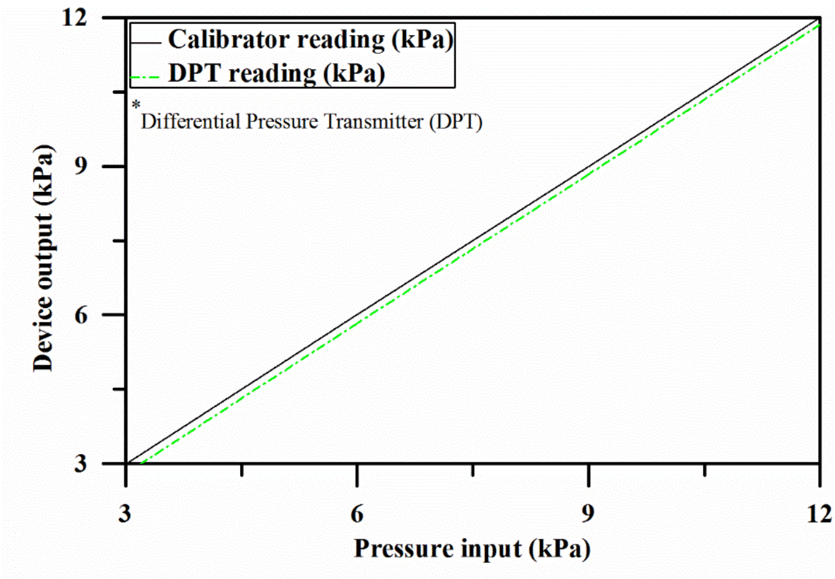

Fig. B1. Calibration curve of the differential pressure transmitter.

In this study, an offset trim was used without a slope trim to adjust the output of a transmitter to compensate for mounting position and line pressure effects. According to the supplier, typically, only an offset trim is required to adjust the calibration of a Rosemount Transmitter in the practical field. An offset trim is an adjustment that shifts the position of the sensor characterisation curve, but it does not affect the slope of the curve. This shift is illustrated in Fig. B1.

Appendix C.

Ultrasonic flow meter calibration procedure

Calibration of the ultrasonic flowmeter was conducted using simple techniques for flow meter calibration. The amount of fluid flow through the pipe of the test section was recorded with respect to time, and compared with the results recorded in the LabVIEW program that corresponds to the data point of volumetric flow rate of the working fluid through the test section. There was very favourable agreement with the manual and LabVIEW measurement data points shown in the Fig. C1.

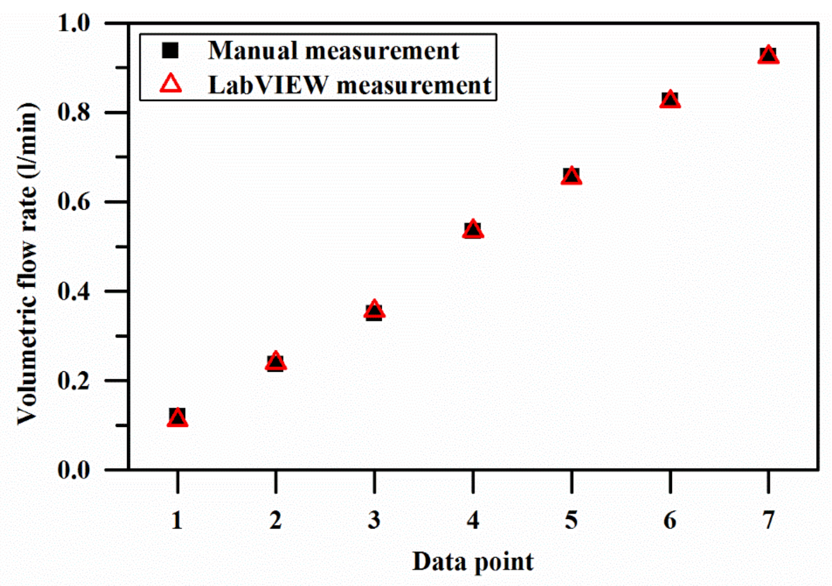

Fig. C1. Comparison of measurement of volumetric flow rate at different data points.

Appendix D.

Certificate of Analysis

Al_2O_3 nanoparticle

Average particle size is 10 nm, ≥99%

Table D1. Inductively Coupled Plasma (ICP) analysis for Al_2O_3 nanoparticle

Components	Contents (ppm)
Ca	≤25
Fe	≤80
Cr	≤3.5
Co	≤2

Given by the supplier

CuO nanoparticle

Average particle size is 30-50 nm, ≥99+%

Table D2. Inductively Coupled Plasma (ICP) analysis for CuO nanoparticle

Components	Contents (ppm)
Ba	0.8
Ca	400
Cd	2.4
Co	6.4
Fe	87
K	300
Mg	72
Mn	3.2
P	300
Pb	100
Sr	2.4
Zn	200

Given by the supplier

References

[1] M.A. Khairul, K. Shah, E. Doroodchi, B. Moghtaderi, Application of nanofluids to enhance heat transfer in renewable energy systems, in: 3rd ASEAN Australian Engineering Congress (AAEC 2015): Australian Engineering Congress on Innovative Technologies for Sustainable Development and Renewable Energy, Engineers Australia, Singapore, 2015, pp. 49-54.

[2] S.M.S. Murshed, K.C. Leong, C. Yang, Thermophysical and electrokinetic properties of nanofluids – A critical review, Applied Thermal Engineering, 28 (2008) 2109-2125.

[3] S.K. Das, S.U.S. Choi, H.E. Patel, Heat Transfer in Nanofluids—A Review, Heat Transfer Engineering, 27 (2006) 3-19.

[4] H.A. Mohammed, K. Narrein, Thermal and hydraulic characteristics of nanofluid flow in a helically coiled tube heat exchanger, International communications in heat and mass transfer, 39 (2012) 1375-1383.

[5] Z. Wu, L. Wang, B. Sundén, Pressure drop and convective heat transfer of water and nanofluids in a double-pipe helical heat exchanger, Applied Thermal Engineering, 60 (2013) 266-274.

[6] J.C. Maxwell, A Treatise on Electricity and Magnetism Dover Publications, Unabriged Third Edition, Volume one, (1954).

[7] W.C. Williams, Experimental and theoretical investigation of transport phenomena in nanoparticle colloids (nanofluids), in, Vol. PhD, Massachusetts Institute of Technology, 2007.

[8] M.A. Khairul, R. Saidur, M.M. Rahman, M.A. Alim, A. Hossain, Z. Abdin, Heat transfer and thermodynamic analyses of a helically coiled heat exchanger using different types of nanofluids, International Journal of Heat and Mass Transfer, 67 (2013) 398-403.

[9] M. Xing, J. Yu, R. Wang, Thermo-physical properties of water-based single-walled carbon nanotube nanofluid as advanced coolant, Applied Thermal Engineering, 87 (2015) 344-351.

[10] B.C. Pak, Y.I. Cho, Hydrodynamic and heat transfer study of dispersed fluids with submicron metallic oxide particles, Experimental Heat Transfer, 11 (1998) 151-170.

[11] Y. Xuan, Q. Li, Investigation on Convective Heat Transfer and Flow Features of Nanofluids, Journal of Heat Transfer, 125 (2003) 151-155.

[12] K.V. Sharma, L.S. Sundar, P.K. Sarma, Estimation of heat transfer coefficient and friction factor in the transition flow with low volume concentration of Al2O3 nanofluid flowing in a circular tube and with twisted tape insert, International communications in heat and mass transfer, 36 (2009) 503-507.

[13] S. Suresh, K.P. Venkitaraj, P. Selvakumar, M. Chandrasekar, A comparison of thermal characteristics of Al2O3/water and CuO/water nanofluids in transition flow through a straight

circular duct fitted with helical screw tape inserts, Experimental Thermal and Fluid Science, 39 (2012) 37-44.

[14] M.T. Naik, S.S. Fahad, L. Syam Sundar, M.K. Singh, Comparative study on thermal performance of twisted tape and wire coil inserts in turbulent flow using CuO/water nanofluid, Experimental Thermal and Fluid Science, 57 (2014) 65-76.

[15] S.M. Fotukian, M. Nasr Esfahany, Experimental study of turbulent convective heat transfer and pressure drop of dilute CuO/water nanofluid inside a circular tube, International communications in heat and mass transfer, 37 (2010) 214-219.

[16] S.M. Fotukian, M. Nasr Esfahany, Experimental investigation of turbulent convective heat transfer of dilute γ-Al2O3/water nanofluid inside a circular tube, International Journal of Heat and Fluid Flow, 31 (2010) 606-612.

[17] K.B. Anoop, T. Sundararajan, S.K. Das, Effect of particle size on the convective heat transfer in nanofluid in the developing region, International Journal of Heat and Mass Transfer, 52 (2009) 2189-2195.

[18] D. Kim, Y. Kwon, Y. Cho, C. Li, S. Cheong, Y. Hwang, J. Lee, D. Hong, S. Moon, Convective heat transfer characteristics of nanofluids under laminar and turbulent flow conditions, Current Applied Physics, 9 (2009) e119-e123.

[19] D. Wen, Y. Ding, Experimental investigation into convective heat transfer of nanofluids at the entrance region under laminar flow conditions, International Journal of Heat and Mass Transfer, 47 (2004) 5181-5188.

[20] S. Zeinali Heris, S.G. Etemad, M. Nasr Esfahany, Experimental investigation of oxide nanofluids laminar flow convective heat transfer, International communications in heat and mass transfer, 33 (2006) 529-535.

[21] J.P. Meyer, T.J. McKrell, K. Grote, The influence of multi-walled carbon nanotubes on single-phase heat transfer and pressure drop characteristics in the transitional flow regime of smooth tubes, International Journal of Heat and Mass Transfer, 58 (2013) 597-609.

[22] S. Kakaç, A. Pramuanjaroenkij, Review of convective heat transfer enhancement with nanofluids, International Journal of Heat and Mass Transfer, 52 (2009) 3187-3196.

[23] A. Amrollahi, A.M. Rashidi, R. Lotfi, M. Emami Meibodi, K. Kashefi, Convection heat transfer of functionalized MWNT in aqueous fluids in laminar and turbulent flow at the entrance region, International communications in heat and mass transfer, 37 (2010) 717-723.

[24] S. Ferrouillat, A. Bontemps, J.-P. Ribeiro, J.-A. Gruss, O. Soriano, Hydraulic and heat transfer study of SiO2/water nanofluids in horizontal tubes with imposed wall temperature boundary conditions, International Journal of Heat and Fluid Flow, 32 (2011) 424-439.

[25] A.J. Ghajar, L.-M. Tam, Heat transfer measurements and correlations in the transition region for a circular tube with three different inlet configurations, Experimental Thermal and Fluid Science, 8 (1994) 79-90.

[26] Y. Ding, H. Alias, D. Wen, R.A. Williams, Heat transfer of aqueous suspensions of carbon nanotubes (CNT nanofluids), International Journal of Heat and Mass Transfer, 49 (2006) 240-250.

[27] D. Liu, L. Yu, Single-Phase Thermal Transport of Nanofluids in a Minichannel, Journal of Heat Transfer, 133 (2010) 031009-031009.

[28] J.A. Olivier, J.P. Meyer, Single-Phase Heat Transfer and Pressure Drop of the Cooling of Water inside Smooth Tubes for Transitional Flow with Different Inlet Geometries (RP-1280), HVAC&R Research, 16 (2010) 471-496.

[29] J.P. Meyer, J.A. Olivier, Transitional flow inside enhanced tubes for fully developed and developing flow with different types of inlet disturbances: Part I – Adiabatic pressure drops, International Journal of Heat and Mass Transfer, 54 (2011) 1587-1597.

[30] M.A. Khairul, K. Shah, E. Doroodchi, R. Azizian, B. Moghtaderi, Effects of surfactant on stability and thermo-physical properties of metal oxide nanofluids, International Journal of Heat and Mass Transfer, 98 (2016) 778-787.

[31] M.A. Khairul, M.A. Alim, I.M. Mahbubul, R. Saidur, A. Hepbasli, A. Hossain, Heat transfer performance and exergy analyses of a corrugated plate heat exchanger using metal oxide nanofluids, International communications in heat and mass transfer, 50 (2014) 8-14.

[32] M.A. Rosen, I. Dincer, M. Kanoglu, Role of exergy in increasing efficiency and sustainability and reducing environmental impact, Energy Policy, 36 (2008) 128-137.

[33] E. Shojaeizadeh, F. Veysi, Development of a correlation for parameter controlling using exergy efficiency optimization of an Al2O3/water nanofluid based flat-plate solar collector, Applied Thermal Engineering, 98 (2016) 1116-1129.

[34] K.V. Sharma, S. L Syam, Laminar convective heat transfer and friction factor of Al_2O_3 nanofluid in circular tube fitted with twisted tape inserts, International Journal of Automotive and Mechanical Engineering, 3 (2011) 265-278.

[35] J. Lienhard IV, A Heat Transfer Textbook, chap. 10, 3rd ed., Phlogiston Press, Cambridge, MA, 2002.

[36] W. Duangthongsuk, S. Wongwises, An experimental study on the heat transfer performance and pressure drop of TiO2-water nanofluids flowing under a turbulent flow regime, International Journal of Heat and Mass Transfer, 53 (2010) 334-344.

[37] F.W. Dittus, L.M.K. Boelter, Heat transfer in automobile radiators of the tubular type, International communications in heat and mass transfer, 12 (1985) 3-22.

[38] R.S. Vajjha, D.K. Das, D.P. Kulkarni, Development of new correlations for convective heat transfer and friction factor in turbulent regime for nanofluids, International Journal of Heat and Mass Transfer, 53 (2010) 4607-4618.

[39] H. Mohammed, H.A. Hasan, M. Wahid, Heat transfer enhancement of nanofluids in a double pipe heat exchanger with louvered strip inserts, International communications in heat and mass transfer, 40 (2012) 36-46.

[40] R. Azizian, E. Doroodchi, T. McKrell, J. Buongiorno, L.W. Hu, B. Moghtaderi, Effect of magnetic field on laminar convective heat transfer of magnetite nanofluids, International Journal of Heat and Mass Transfer, 68 (2014) 94-109.

[41] A. International, P.J. Blau, J.R. Davis, ASM Handbook: Properties and Selection: Irons, Steels, and High-performance Alloys, ASM International, 2001.

[42] M. Shanbedi, S.Z. Heris, M. Baniadam, A. Amiri, M. Maghrebi, Investigation of Heat-Transfer Characterization of EDA-MWCNT/DI-Water Nanofluid in a Two-Phase Closed Thermosyphon, Industrial & Engineering Chemistry Research, 51 (2012) 1423-1428.

[43] M. Voldsund, T.-V. Nguyen, B. Elmegaard, I.S. Ertesvåg, A. Røsjorde, K. Jøssang, S. Kjelstrup, Exergy destruction and losses on four North Sea offshore platforms: A comparative study of the oil and gas processing plants, Energy, 74 (2014) 45-58.

[44] S. Zimmermann, M.K. Tiwari, I. Meijer, S. Paredes, B. Michel, D. Poulikakos, Hot water cooled electronics: Exergy analysis and waste heat reuse feasibility, International Journal of Heat and Mass Transfer, 55 (2012) 6391-6399.

[45] J.A.W. Gut, R. Fernandes, J.M. Pinto, C.C. Tadini, Thermal model validation of plate heat exchangers with generalized configurations, Chemical Engineering Science, 59 (2004) 4591-4600.

[46] J.P. Holman, Experimental methods for engineers, Sixth ed., McGraw-Hill, New York, 1994.

[47] R.W. Allen, E.R.G. Eckert, Friction and heat-transfer measurements to turbulent pipe flow of water (Pr=7 and 8) at uniform wall heat flux, Journal of Heat Transfer, 86 (1964) 301-310.

[48] L.-M. Tam, A.J. Ghajar, Effect of inlet geometry and heating on the fully developed friction factor in the transition region of a horizontal tube, Experimental Thermal and Fluid Science, 15 (1997) 52-64.

[49] B. Shome, M.K. Jensen, Mixed convection laminar flow and heat transfer of liquids in isothermal horizontal circular ducts, International Journal of Heat and Mass Transfer, 38 (1995) 1945-1956.

[50] H. Chen, W. Yang, Y. He, Y. Ding, L. Zhang, C. Tan, A.A. Lapkin, D.V. Bavykin, Heat transfer and flow behaviour of aqueous suspensions of titanate nanotubes (nanofluids), Powder Technology, 183 (2008) 63-72.

[51] A. Tohidi, H. Ghaffari, H. Nasibi, A.S. Mujumdar, Heat transfer enhancement by combination of chaotic advection and nanofluids flow in helically coiled tube, Applied Thermal Engineering, 86 (2015) 91-105.

[52] W. Yu, D.M. France, D.S. Smith, D. Singh, E.V. Timofeeva, J.L. Routbort, Heat transfer to a silicon carbide/water nanofluid, International Journal of Heat and Mass Transfer, 52 (2009) 3606-3612.

[53] S.S. Khaleduzzaman, R. Saidur, I.M. Mahbubul, T.A. Ward, M.R. Sohel, I.M. Shahrul, J. Selvaraj, M.M. Rahman, Energy, Exergy, and Friction Factor Analysis of Nanofluid as a

Coolant for Electronics, Industrial & Engineering Chemistry Research, 53 (2014) 10512-10518.

[54] M. Shanbedi, S. Zeinali Heris, M. Baniadam, A. Amiri, The Effect of Multi-Walled Carbon Nanotube/Water Nanofluid on Thermal Performance of a Two-Phase Closed Thermosyphon, Experimental Heat Transfer, 26 (2013) 26-40.

[55] X. Fang, Y. Xuan, Q. Li, Experimental investigation on enhanced mass transfer in nanofluids, Applied Physics Letters, 95 (2009) 203108.

[56] S. Krishnamurthy, P. Bhattacharya, P.E. Phelan, R.S. Prasher, Enhanced Mass Transport in Nanofluids, Nano Letters, 6 (2006) 419-423.

[57] M. Moghaddami, A. Mohammadzade, S.A.V. Esfehani, Second law analysis of nanofluid flow, Energy Conversion and Management, 52 (2011) 1397-1405.